

# UC Davis

## UC Davis Previously Published Works

### Title

Anthropogenic Extremely Low Volatility Organics (ELVOCs) Govern the Growth of Molecular Clusters Over the Southern Great Plains During the Springtime

### Permalink

<https://escholarship.org/uc/item/4s12b448>

### Journal

Journal of Geophysical Research: Atmospheres, 129(21)

### ISSN

2169-897X

### Authors

Shrivastava, Manish

Zhang, Jie

Zaveri, Rahul A

et al.

### Publication Date

2024-11-16

### DOI

10.1029/2024jd041212

### Copyright Information

This work is made available under the terms of a Creative Commons Attribution License, available at <https://creativecommons.org/licenses/by/4.0/>

Peer reviewed



## RESEARCH ARTICLE

10.1029/2024JD041212

### Key Points:

- Dimethylamines (DMA) and sulfuric acid drive nucleation over the Southern Great Plain (SGP) region in the Midwest USA
- Aromatic low volatile organic gases govern the growth of molecular clusters to larger sizes
- Nucleation in forested regions of southeast USA is limited by sulfuric acid

### Supporting Information:

Supporting Information may be found in the online version of this article.

### Correspondence to:

M. Shrivastava,  
ManishKumar.Shrivastava@pnnl.gov

### Citation:

Shrivastava, M., Zhang, J., Zaveri, R. A., Zhao, B., Pierce, J. R., O'Donnell, S. E., et al. (2024). Anthropogenic extremely low volatility organics (ELVOCs) govern the growth of molecular clusters over the Southern Great Plains during the springtime. *Journal of Geophysical Research: Atmospheres*, 129, e2024JD041212. <https://doi.org/10.1029/2024JD041212>












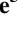


Received 20 MAR 2024

Accepted 7 OCT 2024

© 2024 Battelle Memorial Institute and The Author(s). This article has been contributed to by U.S. Government employees and their work is in the public domain in the USA.

This is an open access article under the terms of the [Creative Commons Attribution-NonCommercial-NoDerivs License](#), which permits use and distribution in any medium, provided the original work is properly cited, the use is non-commercial and no modifications or adaptations are made.

## Anthropogenic Extremely Low Volatility Organics (ELVOCs) Govern the Growth of Molecular Clusters Over the Southern Great Plains During the Springtime

Manish Shrivastava<sup>1</sup> , Jie Zhang<sup>1,2</sup> , Rahul A. Zaveri<sup>1</sup> , Bin Zhao<sup>3</sup> , Jeffrey R. Pierce<sup>4</sup> , Samuel E. O'Donnell<sup>4</sup> , Jerome D. Fast<sup>1</sup> , Brian Gaudet<sup>1</sup> , John E. Shilling<sup>1</sup> , Alla Zelenyuk<sup>1</sup> , Benjamin N. Murphy<sup>5</sup> , Havala O. T. Pye<sup>5</sup> , Qi Zhang<sup>6,7</sup> , Justin Trousdell<sup>6</sup>, Renyi Zhang<sup>8</sup>, Yixin Li<sup>9</sup>, and Qi Chen<sup>10</sup> 

<sup>1</sup>Pacific Northwest National Laboratory, Richland, WA, USA, <sup>2</sup>Now at Lawrence Berkeley National Laboratory, Berkeley, CA, USA, <sup>3</sup>State Key Joint Laboratory of Environmental Simulation and Pollution Control, School of Environment, Tsinghua University, Beijing, China, <sup>4</sup>Department of Atmospheric Science, Colorado State University, Fort Collins, CO, USA, <sup>5</sup>Office of Research and Development, US Environmental Protection Agency, Research Triangle Park, NC, USA, <sup>6</sup>Department of Environmental Toxicology, University of California, Davis, CA, USA, <sup>7</sup>Agricultural and Environmental Chemistry Graduate Group, University of California, Davis, CA, USA, <sup>8</sup>Departments of Atmospheric Sciences and Chemistry, Texas A&M University, College Station, TX, USA, <sup>9</sup>Department of Atmospheric Sciences, Texas A&M University, College Station, TX, USA, <sup>10</sup>State Key Joint Laboratory of Environmental Simulation and Pollution Control, BIC-ESAT and IIRC, College of Environmental Sciences and Engineering, Peking University, Beijing, China

**Abstract** New particle formation (NPF) often drives cloud condensation nuclei concentrations and the processes governing nucleation of molecular clusters vary substantially in different regions. The growth of these clusters from ~2 to >10 nm diameters is often driven by the availability of extremely low volatility organic vapors (ELVOCs). Although the pathways to ELVOC formation from the oxidation of biogenic terpenes are better understood, the mechanistic pathways for ELVOC formation from oxidation of anthropogenic organics are less well understood. We integrate measurements and detailed regional model simulations to understand the processes governing NPF and secondary organic aerosol formation at the Southern Great Plain (SGP) observatory in Oklahoma and compare these with a site within the Bankhead National Forest (BNF) in Alabama, southeast USA. During our two simulated NPF event days, nucleation rates are predicted to be at least an order of magnitude higher at SGP compared to BNF largely due to lower sulfuric acid (H<sub>2</sub>SO<sub>4</sub>) concentrations at BNF. Among the different nucleation mechanisms in WRF-Chem, we find that the dimethylamine (DMA) + H<sub>2</sub>SO<sub>4</sub> nucleation mechanism dominates at SGP. We find that anthropogenic ELVOCs are critical for explaining the growth of particles observed at SGP. Treating organic particles as semisolid, with strong diffusion limitations for organic vapor uptake in the particle phase, brings model predictions into closer agreement with observations. We also simulate two non-NPF event days observed at the SGP site and show that low-level clouds reduce photochemical activity with corresponding reductions in H<sub>2</sub>SO<sub>4</sub> and anthropogenic ELVOC concentrations, thereby explaining the lack of NPF.

**Plain Language Summary** In forested regions around the world, biogenic emissions have been reported to be key drivers of new particle formation (NPF), cloud condensation nuclei (CCN). However, at locations in the Midwest USA that are far from forests and influenced by croplands and urban sources, the processes driving NPF and CCN are not well understood. Using detailed regional model simulations, we show that dimethylamines (DMA) and sulfuric acid (H<sub>2</sub>SO<sub>4</sub>) are key nucleation drivers at the Southern Great Plain (SGP) site during our two simulated days in the springtime, and condensation of H<sub>2</sub>SO<sub>4</sub> alone is not sufficient to explain the observed growth of molecular clusters from ~2 nm diameters to >10 nm diameter. We show that anthropogenic extremely low volatility organics (ELVOCs) are critical for explaining the observed particle growth. In contrast, our simulated non-NPF days at SGP are characterized by low-level clouds, which reduce photochemical activity, H<sub>2</sub>SO<sub>4</sub>, and ELVOC concentrations, thereby explaining the lack of NPF. At the BNF forested site in southeast USA, we show that nucleation rates are limited by availability of H<sub>2</sub>SO<sub>4</sub>. Our study highlights the large heterogeneities in nucleation and particle growth mechanisms within the Midwest compared to southeast USA.

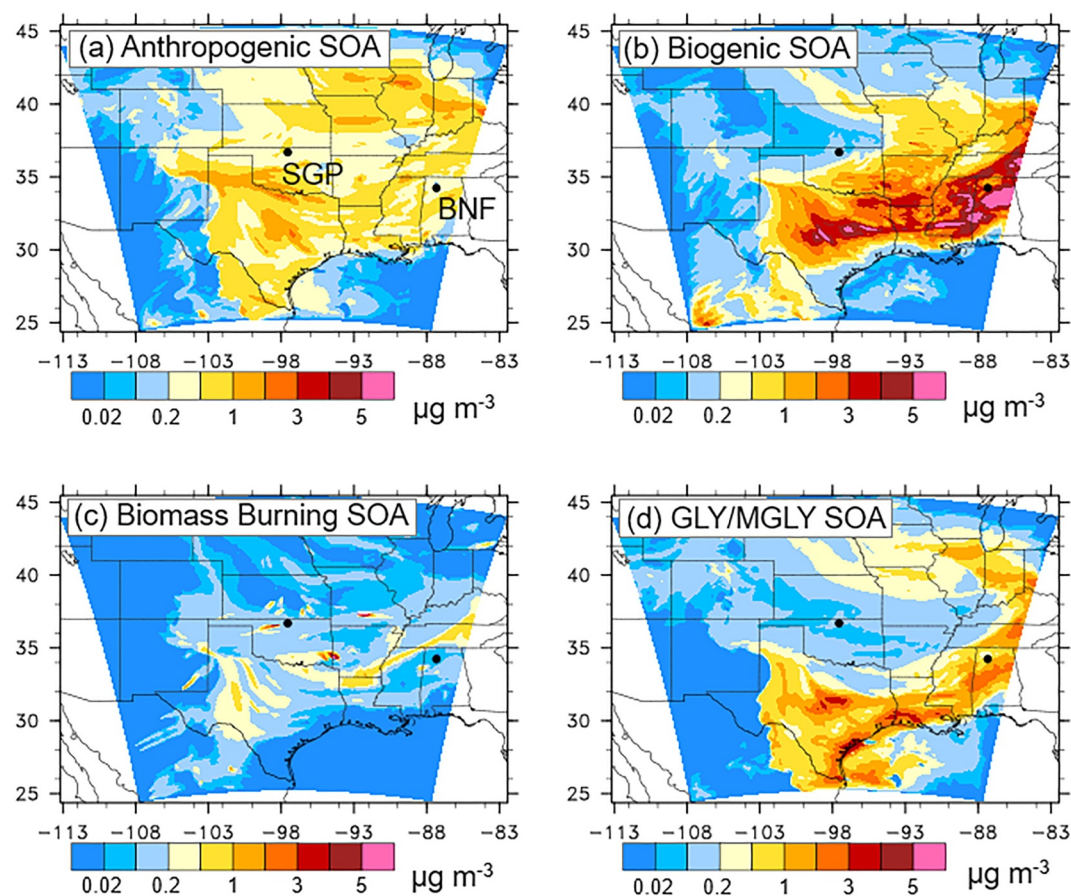
## 1. Introduction

Aerosol particles exert considerable influence on our climate systems through their ability to scatter and absorb sunlight (direct radiative forcing) and by acting as cloud condensation nuclei (CCN), that is, particles on which clouds droplets form (indirect radiative forcing) (Petäjä et al., 2022; Seinfeld et al., 2016; Shrivastava et al., 2017). New particle formation (NPF) is often the major source of CCN in many locations around the world. NPF refers to the nucleation of gaseous precursors such as sulfuric acid, amines, and extremely low volatility organics to form stable clusters followed by the growth of these clusters (Dunne et al., 2016; Ge et al., 2011; Kirkby et al., 2023; Kulmala et al., 2004) to diameters >50 nm where they can serve as CCN. The growth of clusters can occur from multigenerational chemistry and autoxidation processes of organic gases in the atmosphere to form low volatility products that can easily condense on the growing particles.

Over the last decade, the rapid autoxidation of endocyclic alkenes in the gas-phase, initiated by reaction with ozone and OH radicals, has been shown to produce highly oxygenated organic molecules (HOMs) (Ehn et al., 2014; Jokinen et al., 2014; Rissanen et al., 2014), which have low volatilities and could facilitate NPF and growth of molecular clusters. Over high altitudes in the Amazon rainforest, NPF driven by extremely low volatility organics (ELVOCs) from biogenic emissions has been shown to explain the large number of aerosols observed by aircraft (B. Zhao et al., 2020). HOMs are formed in the atmosphere through autoxidation involving peroxy radicals that arise from VOCs. However, ELVOCs are defined through their  $C^*$ ; hence, their definition does not include their formation mechanisms. According to Bianchi et al. (2019), HOMs are primarily ELVOCs (compounds with  $C^* < 3 \times 10^5 \mu\text{g m}^{-3}$ ) but could also include other compound classes in the low volatility (LVOC) and semi-volatile (SVOC) range. Anthropogenic VOCs (AVOCs), consisting of species such as aromatics and alkanes that do not react appreciably with ozone, could also form HOMs due to OH radical initiated autoxidation (Cheng et al., 2024), and the autoxidation/HOM formation potential increases with multigenerational oxidation of AVOCs by OH (Cheng et al., 2024; Garmash et al., 2020; Molteni et al., 2018; Rissanen, 2021; M. Wang et al., 2020; S. N. Wang et al., 2017; Xiao et al., 2021). AVOCs are emitted from several human sources such as vehicles, combustion for energy production, and non-combustion volatile chemical products (VCPs). VCPs are released from solvents, adhesives, paints, lubricants, cosmetics, personal care products, etc., and in addition to combustion derived AVOCs, oxidation of VCPs has been shown to produce significant secondary organic aerosol (SOA) in urban environments (McDonald et al., 2018; Pennington et al., 2021). Due to their complex reaction pathways with OH radicals and the increasing potential of oxidized AVOC products for autoxidation and HOM formation, the specific chemical pathways for AVOC HOM formation are not well understood (Rissanen, 2021). In regions dominated by AVOCs, considerable insights into their HOM formation potential can be gained by analyzing NPF and growth of particles. Especially, in the particle diameter size range of 1–10 nm, ELVOCs help with the early growth rates of freshly nucleated molecular clusters, thereby increasing their survival against coagulation losses with larger aerosols (Shrivastava et al., 2017). At the smallest particle sizes (<10 nm diameter), the Kelvin factor greatly multiplies the equilibrium vapor pressure of organics at the particle surface (R. Zhang et al., 2012); therefore, the least volatile ELVOCs are needed to grow these particles.

To understand the processes governing NPF and growth, we integrate measurements during the Holistic Interactions of Shallow Clouds, Aerosols and Land Ecosystems (HI-SCALE) field campaign (HI-SCALE) 2016 field campaign in the vicinity of the SGP observatory in Oklahoma, USA and three-dimensional regional model simulations with the WRF-Chem model. A previous study simulated NPF and growth over several days during HI-SCALE 2016 field campaign using a 1D column atmospheric model (O'Donnell et al., 2023), which prescribed gas-phase and aerosol parameters near the surface from HI-SCALE measurements but did not account for 3D regional variation emissions, chemistry, and transport processes. Our detailed 3D WRF-Chem model explicitly resolves horizontal and vertical variations of emissions, chemistry, and transport. Here, we analyze four of the days: two NPF event days of 28 April and 14 May 2016 and two non-NPF days of 16 and 19 May 2016, which were characterized by northerly winds identified through observations and column modeling in the previous study (O'Donnell et al., 2023).

Through various WRF-Chem sensitivity simulations, we find that on 28 April 2016, a day characterized by relatively low condensation sinks (CS) and northerly winds, anthropogenic ELVOCs are critical for explaining the observed number size distribution of particles near the surface at the SGP site. In addition, anthropogenic SOA is a key component of submicron SOA mass concentration during the daytime on this day. We also compare our model results over the SGP region to a site located in the southeastern United States at the Bankhead National



**Figure 1.** WRF-Chem simulated secondary organic aerosol (SOA) components over the modeling domain on 28 April 2016 during the daytime at 17 CDT (a) Anthropogenic SOA (b) Biogenic SOA (sum of isoprene, IEPOX and monoterpene SOA) (c) Biomass burning SOA (d) Glyoxal and methylglyoxal SOA formed by aqueous chemistry.

Forest (BNF) in Alabama and find that SOA composition and NPF mechanisms are significantly different between the two sites during the same time period. The deployment of U.S. Department of Energy's (DOE) Atmospheric Radiation and Measurement (ARM) user facility instruments at the BNF site over the next 5 years will provide a wide range of measurements needed to study atmospheric chemistry, NPF, and aerosol growth mechanisms. Although anthropogenic SOA is predicted to be the key SOA component at SGP during our simulated days in the springtime, we find that biogenic SOA components including isoprene epoxydiol SOA (IEPOX-SOA) are the key SOA components at BNF site during the same days.

## 2. Methods

### 2.1. Regional Modeling

#### 2.1.1. Simulating SOA and NPF in WRF-Chem

We used the regional WRF-Chem 4.2 model (Fast et al., 2006; Grell et al., 2005) to simulate trace gases and aerosols during the Spring season (April and May) of 2016 at 10-km grid spacing. The simulations covered a domain of  $2,240 \times 2,240$  km, encompassing most of the central U.S. and parts of the southeastern U.S. (Figure 1 and Table S1 in Supporting Information S1). The CAM-chem global model (Emmons et al., 2020) provided initial and boundary conditions for trace gases and aerosols. The high-resolution rapid refresh (HRRR) reanalysis data was used to provide meteorological initial and boundary conditions (Dowell et al., 2022) as well as the target fields for nudging. Meteorological and chemical conditions were spun up for 72 hr using WRF-Chem followed by the 24-hr simulation for each of the four simulated days of interest in this study.

Gas-phase chemistry is based on the statewide air pollution research center (SAPRC-99) mechanism, which includes 211 reactions of 74 gas phase species, 18 of which are free radicals. Inorganic aerosol chemistry and the evolution of aerosol size distribution and microphysics in WRF-Chem are represented by the model for simulating aerosol interactions and chemistry (MOSAIC) (Zaveri et al., 2008). We represent each particle-phase chemical constituent in WRF-Chem by 20 particle size sections ranging from 1 nm to 10  $\mu\text{m}$  for both interstitial and cloud-borne aerosols. Hourly aerosol and trace gas emissions from sources other than biomass burning and biogenic emissions are derived from the United States Environmental Protection Agency's 2017 National Emissions Inventory (NEI2017). Biogenic volatile organic compound (BVOC) emissions are derived from the latest version of Model of Emissions of Gases and Aerosols from Nature (MEGAN v2.1) recently coupled within the community land model CLM4 (CALM version 4.0) in WRF-Chem (C. Zhao et al., 2016). We represent SOA formed due to the oxidation of BVOCs, including isoprene, monoterpene, and sesquiterpenes using the previously documented volatility basis set (VBS) approaches (Shrivastava et al., 2019; B. Zhao et al., 2020, 2021) that have shown good agreement with field observations. WRF-Chem simulated anthropogenic SOA formation consists of three major components: (a) VOC-SOA formed by oxidation of aromatic VOCs such as toluene and xylene from all sources including VCPs and mobile sources through a 4-product VBS parameterization derived from fitting experimental data of Ng et al. (2007) as documented in Table S2 in Supporting Information S1. (b) VCP-IVOC-SOA: Emissions of VCPs using the VCPy framework developed by Seltzer et al. (2021) with SOA from intermediate volatility VCP emissions as described by Pennington et al. (2021). (c) Vehicular-IVOC-SOA formed by oxidation of IVOCs emitted from vehicular sources. Vehicular IVOC emissions are included in WRF-Chem based on the EPA's Air QUALity TimE Series EQUATES (Foley et al., 2023) platform for Spring 2016 (Table S3 in Supporting Information S1) and are consistent with a recent study that used a decade of laboratory data and a bottom-up approach to derive organic gas emissions in USA (Murphy et al., 2023), as described in the Supplementary Information. Some anthropogenic SOA is also formed by the gas-particle partitioning of primary anthropogenic organic aerosol (POA) and its subsequent aging with OH radicals in the gas-phase and SOA thus formed by evaporation and aging of gas-phase POA is referred to as SVOC-SOA. We assumed POA is semi-volatile with a saturation vapor concentration ( $C^* = 1 \mu\text{g m}^{-3}$ ); however, due to low POA emissions in the vicinity of SGP and BNF, SVOC-SOA is negligible compared to the other three sources. Species with volatilities greater than  $0.1 \mu\text{g m}^{-3}$  (1, 10 and  $100 \mu\text{g m}^{-3}$ ) in the 4-product, VBS are assumed to undergo multigenerational chemistry with OH radicals such that every oxidation with OH decreases their volatility by 1 order of magnitude with a modest (7.5%) increase in mass to account for oxygen added during functionalization similar to Robinson et al. (2007). Additionally, we simulate the aqueous phase chemistry of isoprene epoxydiols (IEPOX) and glyoxal/methylglyoxal leading to SOA formation. We represent IEPOX-SOA including the acid-catalyzed reaction kinetics of IEPOX in particles followed by nucleophilic addition of water and sulfate to form 2-methyltetrols and organosulfates, as described in Shrivastava et al. (2022). Reaction kinetics of IEPOX-SOA were updated based on laboratory measurements as discussed in our recent study (J. Zhang et al., 2023). Glyoxal and methylglyoxal SOA are treated based on a recent experimental study (Y. Li et al., 2021) as described in Figures S1 and S2 and Tables S4 and S5 in Supporting Information S1.

We treat the condensation/evaporation of SOA using a dynamic gas-particle partitioning approach wherein the model calculates the condensation/evaporation of organic gases using a semi-implicit Eulerian approach with adaptive time stepping based on Zaveri et al. (2014). The dynamic gas-particle partitioning approach represents a significant improvement over the instantaneous equilibrium partitioning of SOA mass that was used in previous WRF-Chem SOA configurations (Shrivastava et al., 2011, 2016, 2019, 2022). We optimized the dynamic gas-particle partitioning approach so that it did not add significant computational expense compared to the instantaneous equilibrium partitioning approach. In addition, limitation to gas-particle mass transfer due to organic particle phase diffusion limitations is explicitly accounted for calculations of organic aerosol (OA) viscosity at each grid cell and time step (Rasool et al., 2021).

### 2.1.2. Biomass Burning

We include primary biomass burning emissions for both gases and aerosols from the 2014 Quick Fire Emissions Database (QFED) (Darmenov & da Silva, 2015) version 2.5. In addition to direct primary biomass-burning organic aerosols (BBOA), we simulate biomass burning SOA (BBSOA) formed by the condensation of oxidation products of biomass burning volatile organic gases. The formation of biomass burning SOA is simulated using a new volatility basis set statistical oxidation model (VBS<sub>SOM</sub>) based on Akherati et al. (2020) and

described recently in more detail in Shrivastava et al. (2024). For computational efficiency, primary BBOA is represented by a single semi-volatile species with a  $C^*$  of  $1 \mu\text{g m}^{-3}$ , which is allowed to partition to the gas phase and subsequently reacts with OH radicals forming biomass burning SOA.

### 2.1.3. NPF Mechanisms

We consider eight different nucleation mechanisms in WRF-Chem. Parameterizations of seven nucleation mechanisms, including binary  $\text{H}_2\text{SO}_4\text{-H}_2\text{O}$  neutral and ion-induced mechanisms, ternary  $\text{H}_2\text{SO}_4\text{-NH}_3\text{-H}_2\text{O}$  neutral and ion-induced mechanisms, pure-organic neutral and ion-induced mechanisms, and the binary organic- $\text{H}_2\text{SO}_4$  mechanism are documented in B. Zhao et al. (2020), whereas the eighth mechanism is  $\text{DMA} + \text{H}_2\text{SO}_4$  nucleation, as described in Y. Li et al. (2023). Newly formed particles are assumed at 1.4 nm for  $\text{DMA} + \text{H}_2\text{SO}_4$  nucleation and 1.7 nm for other nucleation mechanisms, as documented in Y. Li et al. (2023). Gas-phase  $\text{H}_2\text{SO}_4$  concentration is simulated within WRF-Chem through both gas-phase oxidation of  $\text{SO}_2$  by OH radicals in its lumped gas-phase chemistry mechanism (SAPRC-99) and aqueous phase oxidation of S(IV) in cloud droplets to form S(VI).

We distinguished neutral and ion-induced nucleation rates for binary  $\text{H}_2\text{SO}_4\text{-H}_2\text{O}$  nucleation, ternary  $\text{H}_2\text{SO}_4\text{-NH}_3\text{-H}_2\text{O}$  nucleation, and pure-organic nucleation. The nucleation rate parameterizations for these nucleation mechanisms were derived from CLOUD chamber experiments, which were conducted under both neutral (ion-free) and galactic cosmic rays (GCRs). The ion-induced nucleation rates were estimated using the difference between GCR and neutral nucleation rates; therefore, there is no double counting between neutral and ion-induced nucleation rates. The ionization rates were taken from Dunne et al. (2016). Then, the ion concentrations were calculated based on ionization rate, the recombination coefficient, and the loss rate of ions due to scavenging and to ion-induced nucleation itself, following Dunne et al. (2016).

Within the organic mediated NPF mechanisms, the organics participating in nucleation include the ultralow volatility organics (ULVOCs) and ELVOCs formed by oxidation of monoterpenes (Schervish & Donahue, 2020), which we simulate using the WRF-Chem/Radical 2D-VBS (R2D-VBS) model developed in our previous studies (Y. Li et al., 2023; B. Zhao et al., 2020, 2021). The R2D-VBS systematically simulates the temperature-dependent oxidation chemistry of monoterpenes, including the formation of ULVOC and ELVOC. For implementation into a detailed regional model such as WRF-Chem where computational costs greatly increase with simulated number of advected tracers, the R2D-VBS was mapped on to an equivalent 1D-VBS. However, only species with  $\text{O}:\text{C} > 0.4$  were included in this 1D-VBS and the total organic concentrations in the ULVOC and ELVOC ranges of the condensed 1D-VBS were used to drive organic-mediated nucleation. The remaining less-oxygenated compounds (with  $\text{O}:\text{C} \leq 0.4$ ) do not contribute to nucleation in the model formulation.

For the  $\text{DMA} + \text{H}_2\text{SO}_4$  nucleation mechanism, we include the DMA emissions sources in WRF-Chem. DMA emissions vary with source types, and in this work, we estimate DMA emissions based on their reported ratio to  $\text{NH}_3$  (0.0015), which corresponds to agricultural regions and is close to the lower bound of the range of ratios reported by Y. Li et al. (2023). The assumed ratio of DMA to  $\text{NH}_3$  of 0.0015 represents a lower bound emissions ratio corresponding to agricultural regions, while the upper bound ratio of 0.007 corresponds to chemical-industrial sources and is 5 times higher than our assumed ratio, as documented by Y. Li et al. (2023). As discussed later and shown in Figure S17 in Supporting Information S1, changing the DMA emissions ratio does not affect the main results and conclusions of this work regarding the role of DMA, anthropogenic ELVOCs and  $\text{H}_2\text{SO}_4$  on NPF and growth in the vicinity of the SGP site.

Since DMA emissions are based on their ratios with  $\text{NH}_3$  gas, it is important to evaluate WRF-Chem simulated  $\text{NH}_3$  with observations. In our previous study, we evaluated our WRF-Chem predictions of  $\text{NH}_3$  with aircraft measurements on 14 May 2016 in the vicinity of the SGP site during the HI-SCALE field campaign using the chemical ionization mass spectrometer (CIMS) (Schobesberger et al., 2023). Within the boundary layer, WRF-Chem predicted  $\text{NH}_3$  gas concentrations of 1.2–1.4 ppbv agreed with the observed  $\text{NH}_3$  range (using CIMS) of 1.1–2.4 ppbv, as discussed in Figure 6b of Schobesberger et al. (2023).

We also simulate the sinks of DMA in WRF-Chem that include DMA chemical loss by gas-phase reaction with OH radicals (with OH reaction rate constant of  $6.5 \times 10^{-11} \text{ molecule cm}^{-3}$ ) and loss of DMA through its irreversible uptake by aerosols with an assumption of a DMA uptake coefficient of 0.001 (Y. Li et al., 2023; Mao

et al., 2018). The uptake coefficient is a median value corresponding to a range of uptake coefficients determined from field measurements.

#### 2.1.4. ELVOCs From Oxidation of Anthropogenic and Biomass Burning Emissions

The presence of ELVOCs in anthropogenic (Cheng et al., 2024; Garmash et al., 2020; Molteni et al., 2018; Rissanen, 2021; S. N. Wang et al., 2017) and biomass burning SOA (Brege et al., 2021; Shetty et al., 2023) has been previously reported in the literature.

Figure S3 in Supporting Information S1 shows, as an example, single particle measurements of room-temperature evaporation kinetics for different SOA types measured in the PNNL environmental chamber (J. Wang et al., 2019). The figure shows that anthropogenic toluene SOA particles have low volatility, like that of  $\alpha$ -pinene SOA with a nonvolatile fraction (in the ELVOC range) of  $\sim 40\%$ . Laboratory and field measurements indicate the presence of ELVOCs in biomass burning OA particles (Brege et al., 2021; Shetty et al., 2023); however, the gas-phase yields of ELVOCs from oxidation of biomass burning VOCs are lacking. Recently, Shrivastava et al. (2024) presented a case study where gas-phase ELVOCs formed by the oxidation of organic gases emitted by biomass burning fires could promote the growth of newly formed particles, explaining aircraft measurements of ultrafine particles in vegetation fire smoke over the Amazon rainforest.

Since the formation of ELVOCs generated from the oxidation of combustion-derived VOCs (anthropogenic and biomass burning) lacks mechanistic information needed for implementation in a regional model, we estimate the formation of combustion derived ELVOCs assuming that the lowest volatility secondary organic gases corresponding to the  $C^*$  of  $0.01 \mu\text{g m}^{-3}$  in our 4-product VBS (with  $C^*$  of 0.01, 1, 10 and  $100 \mu\text{g m}^{-3}$ ) are transformed to ELVOCs ( $C^*$  of  $10^{-5} \mu\text{g m}^{-3}$ ) instantly within the model chemistry time step of 5 min. Note that the organic gases with the lowest volatility  $C^* = 0.01 \mu\text{g m}^{-3}$  correspond to mostly functionalized species generated by multigenerational oxidation of VOCs, IVOCs, and SVOCs with OH radicals. Our assumption of the  $C^*$  of  $0.01 \mu\text{g m}^{-3}$  species forming ELVOCs is consistent with previous studies showing that the autoxidation/HOM formation potential of AVOCs increases with their multigenerational oxidation by OH radicals (Cheng et al., 2024; Garmash et al., 2020; Molteni et al., 2018; Rissanen, 2021; J. Wang et al., 2017). These combustion derived ELVOCs are assumed to only condense onto preexisting nucleated clusters and particles but are not included in any nucleation scheme due to lack of understanding of their nucleation mechanisms.

To investigate how ELVOCs from different sources affect WRF-Chem simulated NPF and particle size distribution evolution, we compare the following sensitivity simulations: (a) default: includes ELVOCs from all sources (anthropogenic, biogenic, and biomass burning), (b) no Anthro ELVOC: includes ELVOCs from biogenic and biomass burning but excludes anthropogenic ELVOCs, (c) no BiomBurn ELVOCs: includes ELVOCs from biogenic and anthropogenic sources but excludes biomass burning ELVOCs, and (d) no Anth/BB ELVOCs (just biogenic ELVOCs): excludes ELVOCs from anthropogenic and biomass burning sources but includes biogenic monoterpene ELVOCs. Note that we use advanced NPF and SOA modules within WRF-Chem to resolve the aerosol number size distribution, which requires including several species of organic oxidation products encompassing their volatility distributions and a 20-size bin sectional aerosol size distribution (ranging 1 nm to 10  $\mu\text{m}$  diameter particle sizes). Representing this evolution of aerosol number size distribution from their nucleation (at  $\sim 1.4$ – $1.7$  nm diameters) to their growth to sizes relevant for CCN requires advecting a large number of tracers ( $\sim 1,000$ ) in WRF-Chem. Therefore, our simulations are computationally expensive compared to aerosol models that mostly focus on predicting particle mass (requiring fewer advected species) rather than number. Due to the large associated computational costs, we simulate selected observationally identified NPF event and nonevent days at SGP as documented in O'Donell et al. (2023) to gain insights about the atmospheric conditions causing NPF.

### 3. Results

While the HI-SCALE 2016 field campaign was conducted in the vicinity of the SGP site in Oklahoma, future long-term ARM measurements are planned within the Bankhead National Forest in northern Alabama. The southeastern U.S. is characterized by significantly larger biogenic influence and related SOA formation compared to the SGP site. Although BNF measurements are not yet available, we contrast WRF-Chem simulations of NPF and SOA at the SGP and BNF sites to understand the heterogeneities in SOA and NPF mechanisms in these two different environments.

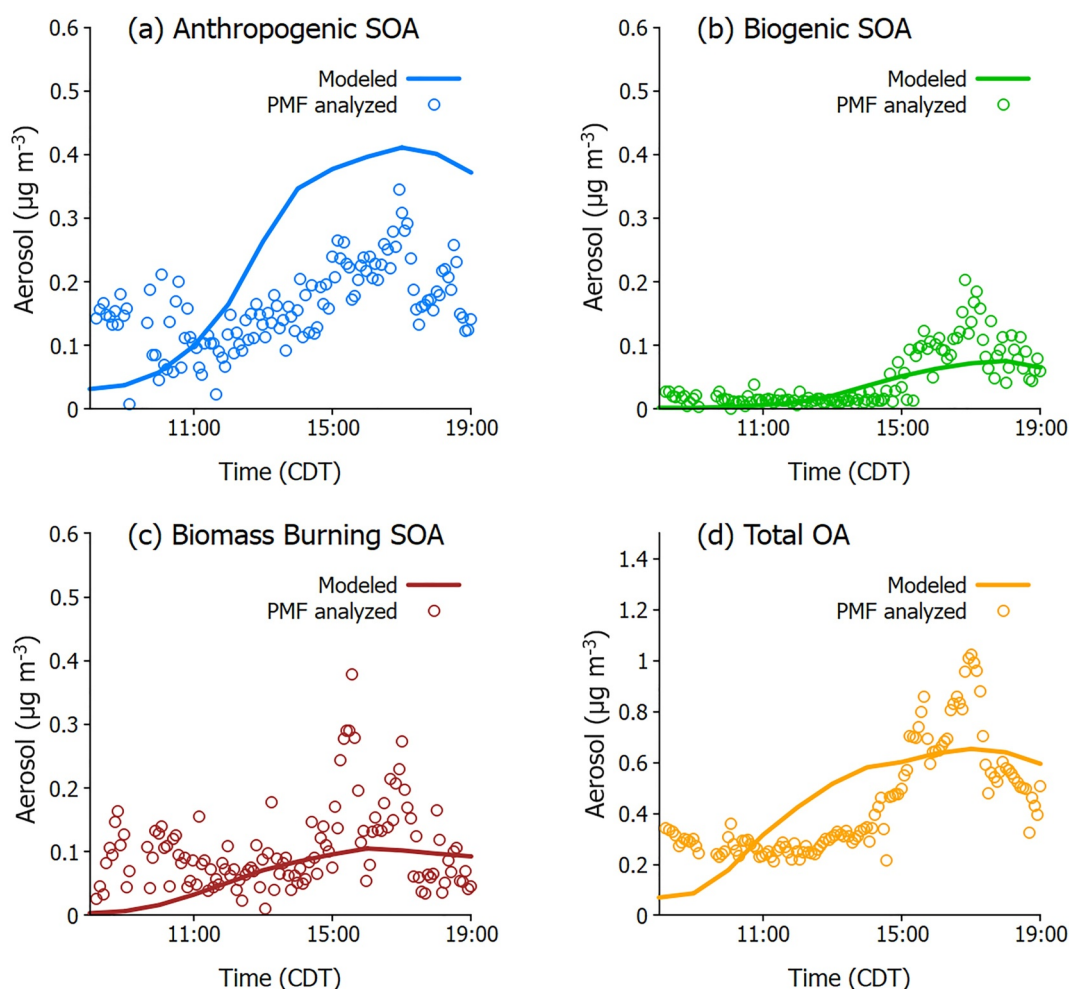
During the HI-SCALE 2016 field campaign, the spring intensive observation period (IOP1, April–May 2016) showed many NPF events. In this study, we select two representative days when NPF was observed at the SGP site: 28 April and 14 May 2016 (O'Donnell et al., 2023). On both days, airmasses largely originate from the north prior to arriving at the SGP site and encountered grasslands, croplands, and some urban influences. These days were also characterized by relatively low CS favoring NPF (O'Donnell et al., 2023). Figure 1 shows that at the SGP site, most of the simulated SOA was anthropogenic SOA (Figure 1a) during the daytime on 28 April, whereas at the BNF site, biogenic SOA (Figure 1b) and glyoxal/methylglyoxal SOA (Figure 1d) were prevalent. Although simulated anthropogenic SOA levels are similar at SGP and BNF sites, the concentration of biogenic SOA is significantly lower at SGP than at BNF, resulting in lower aerosol concentrations and associated CS at SGP.

We evaluated WRF-Chem simulated SOA components with corresponding factors derived from PMF analyses of mass spectral data acquired with a high-resolution time-of-flight aerosol mass spectrometer (HR-AMS) at the SGP surface site (additional details about the PMF results are provided in the supplementary materials). Due to low OA concentrations approaching AMS detection limits (of  $\sim 0.1 \mu\text{g m}^{-3}$ ), uncertainties arise in source apportionment of organic aerosols through PMF. In addition, we note that AMS only measures particles  $>70 \text{ nm}$  in diameter (due to limitations in transmission through its aerodynamic lens) and does not measure particle chemical composition in the size range ( $<20 \text{ nm}$  particle diameter) where ELVOCs are important for particle growth. Therefore, a comparison with AMS data can only serve as a qualitative evaluation of the model for the SOA sources contributing to NPF and growth in the vicinity of SGP. During the daytime of 28 April 2016, both model and measurements show low total OA concentrations (Figure 2d) peaking at  $\sim 0.7 \mu\text{g m}^{-3}$ , which are associated with low CS.

Compared to the AMS PMF factors, the model overpredicts anthropogenic SOA (Figure 2a) and underpredicts biogenic SOA (Figure 2b) by up to a factor of 2; however, the model agrees with measured total organic aerosol (Figure 2d). Both model and measurements also suggest some influence of biomass burning organic aerosol (Figure 2c). As shown in Figure S4b in Supporting Information S1, WRF-Chem predicts that aromatic VOC-SOA formed by oxidation of species such as toluene, xylene with OH radicals is the key anthropogenic SOA type ( $>0.5 \mu\text{g m}^{-3}$ ), whereas VCP and vehicular IVOC-SOA contributions are lower (Figure S4c and S4d in Supporting Information S1,  $\sim 0.2\text{--}0.4 \mu\text{g m}^{-3}$ , respectively). According to PMF analysis, the deconvolved biogenic SOA is typically lower than anthropogenic SOA by approximately a factor of 2 on 28 April 2016, whereas the contribution of biomass burning SOA is much smaller and shows significant scatter (Figure 2c). In agreement with AMS data, single particle composition measurements onboard the DOE G-1 aircraft on 28 April (and 14 May) showed a prevalence of sulfate-rich particles internally mixed with organics, indicating the anthropogenic origins of OA on these days (Saliba et al., 2023). These single particle measurements also suggested minor contributions of biomass burning organic aerosol on both 28 April and 14 May consistent with WRF-Chem predictions. On 14 May, Figure S5a in Supporting Information S1 shows that the model underpredicts anthropogenic SOA in the early morning (before 15 CDT) but it captures the peak anthropogenic SOA loading in the late afternoon consistent with the AMS PMF anthropogenic SOA factor. The model also underpredicts biogenic SOA by more than a factor of 2 (Figure S5b in Supporting Information S1) and predicts a complete absence of biomass burning organic aerosol on 14 May (Figure S5c in Supporting Information S1), whereas the AMS PMF factor shows some biomass burning organic aerosol influence (but with a lot of scatter) suggesting biomass burning organic aerosol concentrations approaching the detection limits of AMS. Although both 28 April and 14 May are characterized by northerly winds (O'Donnell et al., 2023), AMS measurements and WRF-Chem simulations imply that OA sources profiles near the surface at SGP may be different between these days. However, as discussed above, since the AMS does not measure ultrafine particle composition (particle diameters below  $70 \text{ nm}$ ), the above comparisons for sources of OA are qualitative and cannot be used to infer the sources of ELVOCs needed for NPF at SGP. Single particle measurements onboard the aircraft implied greater fraction of sulfate-rich organic particles on 14 May compared to 28 April, indicating greater likelihood of anthropogenic contributions to SOA on 14 May compared to 28 April. As discussed in this manuscript, the growth of nucleated particles with particle diameters  $<2\text{--}30 \text{ nm}$  provides useful constraints about the ELVOCs needed for explaining the observed time evolution of particle size distribution.

AMS measurements were not available for model evaluation at the BNF site; however, the large simulated biogenic SOA contribution at BNF is consistent with the site's forested location and field measurements in SE USA showing the prevalence of biogenic SOA at other rural sites (Chen et al., 2020). Due to the differing SOA





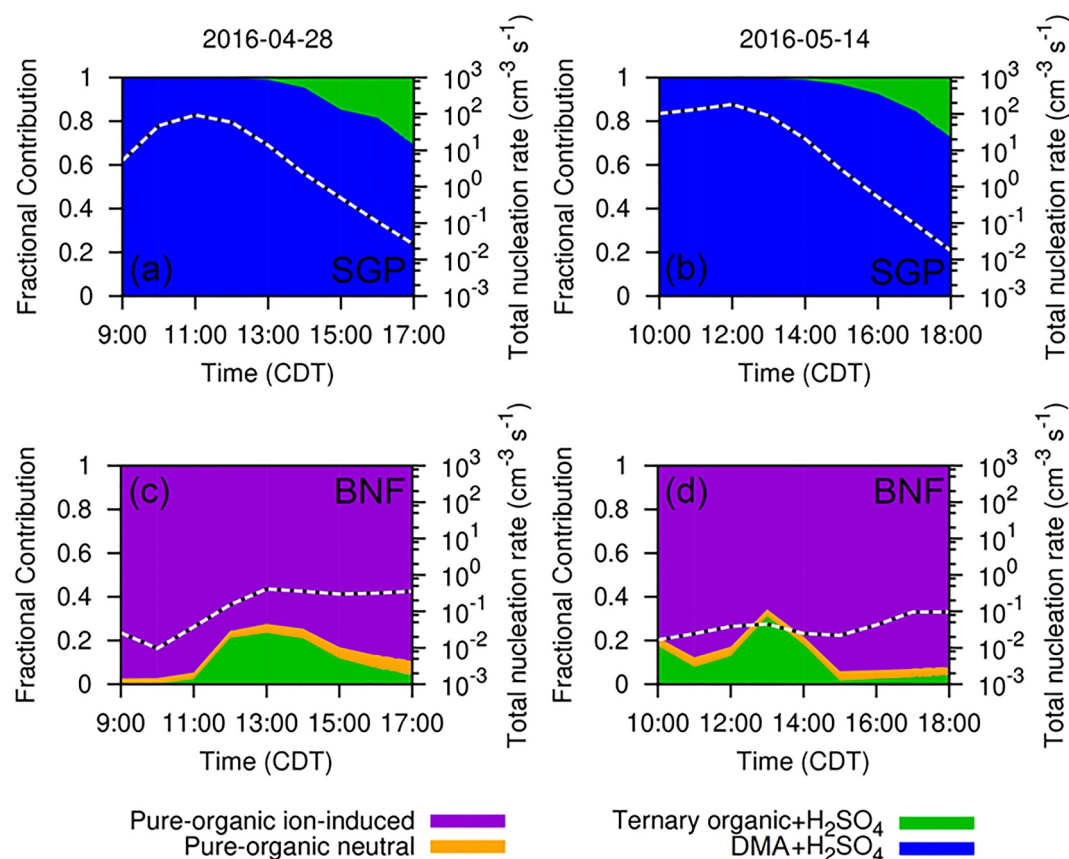
**Figure 2.** WRF-Chem simulated and observed secondary organic aerosol components derived from positive matrix factorization (PMF) of aerosol mass spectrometer (AMS) data at the SGP surface site during the daytime hours on 28 April 2016.

magnitudes, the nucleation rates and mechanisms are expected to be different between SGP and BNF sites as discussed in the following section.

### 3.1. Differences in Nucleation Rates and Mechanisms at SGP and BNF Surface Sites

Figure 3 shows that the near surface WRF-Chem simulated peak nucleation rates (white dashed lines, right y-axes) during the daytime of  $\sim 10\text{--}100\text{ cm}^{-3}\text{ s}^{-1}$  at the SGP site (top panels) and BNF (bottom panels) on both 28 April and 14 May 2016. Peak nucleation rates at the SGP site are  $\sim 2$  orders of magnitude higher than those simulated at the BNF site ( $0.1\text{--}1.0\text{ cm}^{-3}\text{ s}^{-1}$ ). At the BNF site, simulated  $\text{H}_2\text{SO}_4$  concentrations are  $\sim$  an order of magnitude lower than SGP (Figure S6b in Supporting Information S1 and compare orange lines in Figure 8c at SGP vs. Figure S19b in Supporting Information S1 at BNF on 28 April) that are mainly responsible for the low nucleation rates simulated at BNF compared to SGP (as discussed at the end of this section). In addition, the order of magnitude larger simulated CS at the BNF site compared to SGP during the morning at both sites (Figure S7 in Supporting Information S1) partly explains the relatively high nucleation rates at SGP. Increasing CS scavenges the clusters and condensable low volatility precursors that reduce NPF and growth. Higher SOA formation over the BNF site (biogenically dominated) compared to SGP (anthropogenically influenced with a much lower biogenic influence than BNF, as discussed in the preceding section) causes the higher CS at BNF.

At the SGP site, the  $\text{DMA} + \text{H}_2\text{SO}_4$  mechanism (blue, top panels, Figure 3) is the dominant contributor ( $>80\%$ ) to simulated nucleation rates that peak around 11–12 CDT on both days 28 April and 14 May, whereas the low

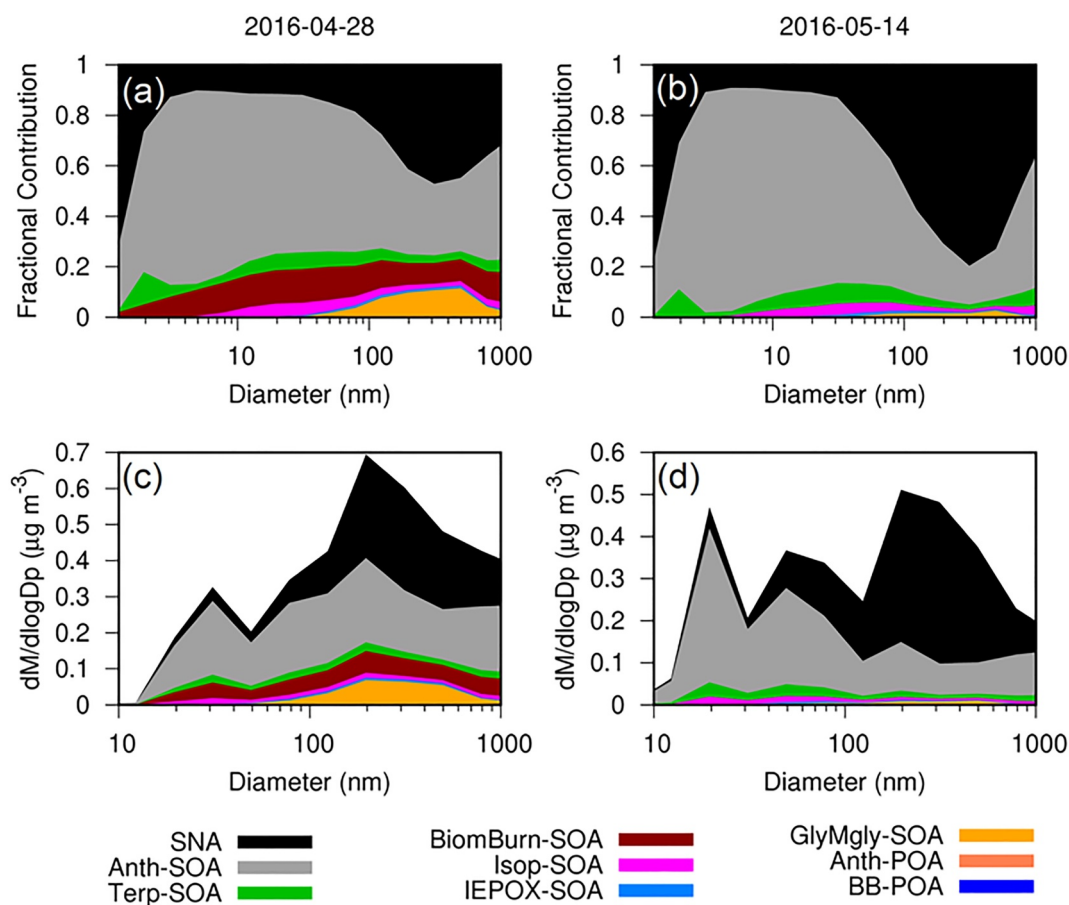


**Figure 3.** WRF-Chem simulated time evolution of total nucleation rates (white dashed lines and right y-axes) and contributions of the top four dominant nucleation mechanisms (out of eight) at the SGP surface site in Oklahoma on two representative days in 2016: 28 April (left panel) and 14 May (right panel).

nucleation rates at the BNF site are primarily pure organic ion-induced nucleation (Figure 3, bottom panels). The simulated peak in nucleation rates at the SGP site on 28 April coincides with low simulated CS (Figure S7 in Supporting Information S1,  $CS \sim 10^{-3} s^{-1}$ ) before 11 CDT that favor nucleation, but the nucleation rate drops as CS increases by a factor of 4 in the late afternoon. The ternary organic +  $H_2SO_4$  contributes up to 20% to the simulated nucleation rate at both SGP and BNF sites on both days. In summary, total nucleation rates are much higher at the SGP site compared to BNF on both days, and the peaks in nucleation rates are mostly explained by the DMA +  $H_2SO_4$  nucleation mechanism at the SGP site. The contribution of DMA +  $H_2SO_4$  mechanism is negligible at the BNF site mostly due to an order of magnitude lower simulated  $H_2SO_4$  concentration at the forested BNF site due to the absence of local  $SO_2$  emissions (causing  $H_2SO_4 < 10^{-5}$  molecule  $cm^{-3}$ ) compared to SGP ( $H_2SO_4$  concentrations  $\sim 2 \times 10^6$  molecule  $cm^{-3}$ ) although DMA concentrations are predicted to be higher at BNF compared to SGP during the early morning (compare orange lines in Figure 8e at SGP vs. Figure S19d in Supporting Information S1 at BNF). In agreement with WRF-Chem,  $H_2SO_4$  concentrations measured by the CIMS onboard the DOE G-1 aircraft were  $\sim 0.1$  pptv approaching the instrument detection limit over the SGP site during our simulated days. WRF-Chem predicts that the relatively low nucleation rates at BNF are most attributed to the pure organic ion-induced and ternary organic +  $H_2SO_4$  nucleation mechanisms.

### 3.2. SOA: A Vital Link Between Nucleation and Growth

SOA is a vital link between nucleation of molecular clusters (formed by nucleation with  $\sim 1.4$ – $1.7$  nm diameter in WRF-Chem) and their growth to CCN relevant sizes (Riipinen et al., 2011; Shrivastava et al., 2017), and during late afternoon anthropogenic SOA contributes  $>70\%$  to simulated ultrafine ( $<100$  nm) aerosol mass at SGP (Figure 4) on both 28 April and 14 May 2016. In contrast, biogenic SOA dominates ultrafine aerosol mass at the BNF site (Figure S8 in Supporting Information S1). At the SGP site, within larger particles in the accumulation



**Figure 4.** WRF-Chem simulated size resolved particle chemical composition at the SGP site during the afternoon at 17 CDT on 28 April 2016 (left panels) and 14 May 2016 (right panels). Top panels are fractional contributions of inorganic and organic components to particle mass, whereas bottom panels are lognormal distributions of simulated mass concentrations ( $dM/d\log D_p$ ). SNA represents the sum of inorganic components including sulfate, nitrate and ammonium. Different OA components indicated in the legends are Anth-SOA: Total anthropogenic secondary organic aerosol (SOA), Terp-SOA: Monoterpene SOA, BiomBurn-SOA: biomass burning SOA, Isop-SOA: Isoprene SOA formed by partitioning to organic phase, IEPOX-SOA formed by multiphase chemistry of IEPOX, GlyMgly-SOA: sum of glyoxal and methylglyoxal SOA, Anth-POA: Anthropogenic primary organic aerosols, and BB-POA: biomass burning primary organic aerosols.

mode (100–500 nm), inorganic aerosols (sulfate and nitrate ammonium) are also predicted to contribute significantly (>20%) to aerosol mass as shown in Figure 4. The predicted inorganic aerosol contribution is higher on 14 May compared to 28 April. As shown in Figure 4 and Figure S8 in Supporting Information S1, the SGP site experiences much lower contributions of biogenic SOA components (terpene SOA, isoprene SOA, glyoxal/methylglyoxal SOA) compared to BNF.

### 3.3. Observed and Simulated NPF and Growth at the SGP Site

At particle diameters <10 nm, the size-dependent Kelvin term decreases the growth of molecular clusters by increasing the equilibrium vapor pressure that governs condensation/evaporation of organic gases to particles (R. Zhang et al., 2012). For example, with an assumed surface tension of organics of 0.05 N/m (Li & Bourq, 2023), molecular weight of 0.25 kg mol<sup>-1</sup>, the Kelvin term for a freshly nucleated 2 nm diameter particle increases the equilibrium vapor pressure of condensable organic gases by a factor of 4,500. Therefore, only species with extremely low volatility (e.g., sulfuric acid and ELVOCs with  $C^* < 3 \times 10^{-5} \mu\text{g m}^{-3}$ ) that could overcome the Kelvin barrier would be able to condense on clusters of ~2 nm sizes (Bianchi et al., 2019; Ehn et al., 2014, 2017; Rissanen, 2021). Quantification of gas-phase HOMs yields through OH-initiated oxidation of VOCs emitted from anthropogenic and biomass burning sources is still lacking (Rissanen, 2021). Using WRF-Chem sensitivity simulations for our simulated days (28 April and 14 May 2016), we show that at the SGP site, sulfuric acid

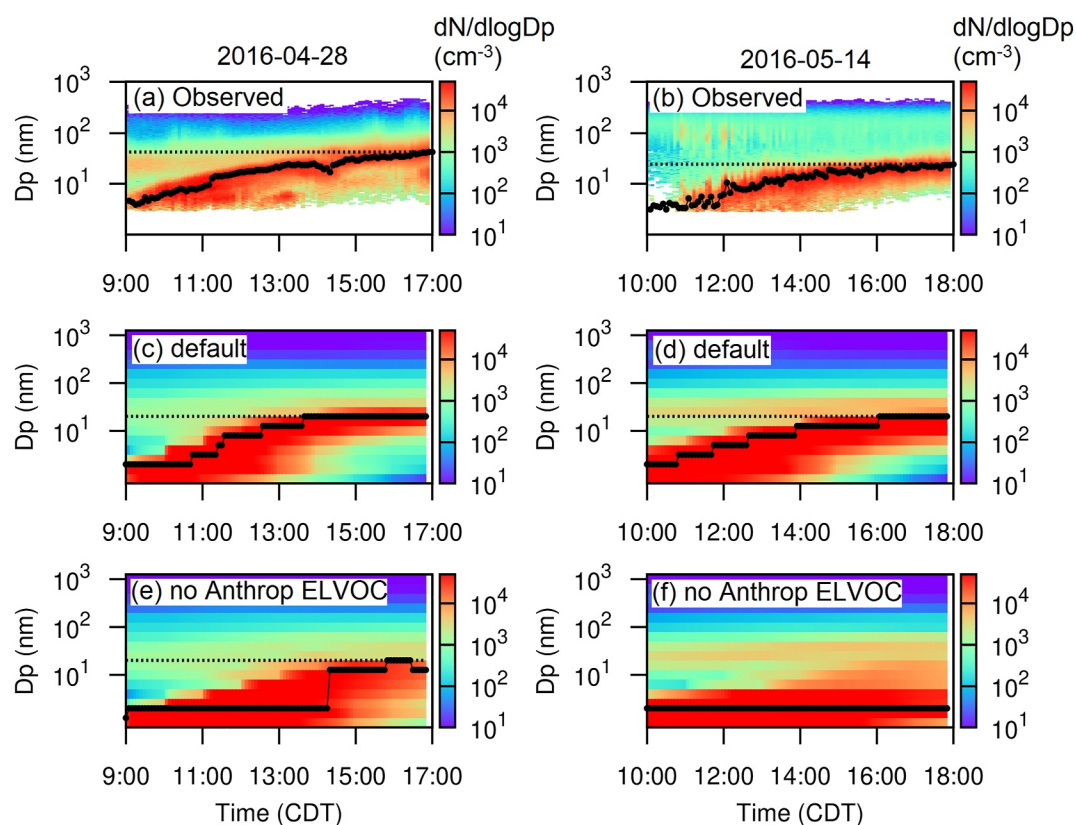
condensation alone is not sufficient to explain the observed growth (Figure 4, top panels), and anthropogenic ELVOCs are needed to grow the nucleated clusters across the Kelvin barrier and to explain the observed time evolution of particle size distributions. During the HI-SCALE 2016 field campaign, measured particle size distributions at the SGP surface site in the range of 2.89–60 nm (nano SMPS) and 11–460 nm (SMPS) (Uin et al., 2019) were used to derive merged size distributions over the range of 2.89–460 nm.

Figure 5 compares the observed (Figures 5a and 5b) and WRF-Chem simulated evolution of particle size distributions at the SGP site. The default model (Figures 5c and 5d), which includes all ELVOCs from biogenic, anthropogenic, and biomass burning sources, shows good agreement with the observed growth of particles (diameters corresponding to peak  $dN/d\log D_p$  indicated by horizontal black lines). WRF-Chem simulated anthropogenic ELVOCs range 1–5 pptv ( $<10^8$  molecule  $\text{cm}^{-3}$ , as shown in Figure 8d) in the early morning over SGP and are in the range of ELVOC concentrations resulting from the oxidation of aromatic VOCs like toluene as measured in laboratory (Cheng et al., 2021, 2024) and field studies (Guo et al., 2022). Turning off the anthropogenic ELVOC source within the noAnthropELVOC simulation greatly reduces the growth of particles (Figures 5e and 5f), and simulated final diameters (shown by dashed horizontal lines) in late afternoon are smaller than observations (Figures 5a and 5b).

As discussed earlier, the noAnthropELVOC simulation still includes ULVOCs and ELVOCs from biogenic monoterpene oxidation products simulated by the R2D-VBS (condensed to a 1D VBS in WRF-Chem) and biomass burning ELVOCs. However, due to low WRF-Chem simulated monoterpene concentrations ( $<0.01$  ppbv) and small monoterpene SOA contributions at the SGP site (Figure 4) (in addition to low biomass burning ELVOCs), the noAnthropELVOC simulation predicts that just the biogenic and biomass burning ELVOCs are not sufficient to simulate the observed particle growth.

Consistent with low monoterpene concentrations simulated in WRF-Chem, measurements with the ground-based proton transfer reaction mass spectrometer (PTR-MS) show that monoterpene concentrations at the SGP site on 28 April during the daytime were on average  $\sim 0.02$  ppb, approaching their lower instrument detection limits. In addition, WRF-Chem simulated concentrations of isoprene oxidation products (IEPOX and ISOPOOH) are low ( $<0.1$  ppb) and agree with the CIMS measurements on board the G-1 aircraft in the vicinity of the SGP site (Figure S9 in Supporting Information S1). Note that measured concentrations of biogenic VOCs by PTR-MS at the SGP site were negligible (0.046 ppbv for isoprene and 0.005–0.01 ppbv for monoterpenes), as documented in Table 1 of O'Donnell et al. (2023), which approach the instrument limit of detection (LOD) of the PTR-MS. Data reported in Table 1 of O'Donnell et al. (2023) are average VOC concentrations over several hours in order to increase the signal-to-noise ratio; however, some values were still at or below the instrument LOD after averaging and were replaced with  $0.5 \times \text{LOD}$ . Considering the averaging and replacement methods employed in O'Donnell et al. (2023), the PTR-MS data reported in their Table 1 should be taken as an “upper bound” for VOC concentrations, as the actual VOC concentrations could be considerably lower. WRF-Chem simulations predict even lower concentrations of isoprene and monoterpenes at the SGP site compared to PTR-MS indicating some degree of model skill; however, a comparison between WRF-Chem and the PTR-MS would be misleading due to the limitations of the PTR-MS data. Therefore, we found it more useful to compare our model to isoprene oxidation products measured by CIMS. In comparison, anthropogenic VOCs measured by PTR-MS were an order of magnitude higher (sum of measured benzene, trimethylbenzene, toluene, and m-xylene of  $\sim 0.15$  ppbv). WRF-Chem simulated concentration of these aromatic VOCs (sum of ARO1 and ARO2 aromatics in SAPRC-99 mechanism within WRF-Chem) are  $\sim 0.27$  ppbv, a factor of 1.8 higher than measurements. We note that the oxidation of ARO1 and ARO2 precursors constitute the largest simulated sources of anthropogenic SOA at the SGP site (Figure S4 in Supporting Information S1).

On 28 April at the SGP site, measurements show that nucleation occurs early in the morning at 9:30 CDT with a peak in particle size distribution of  $\sim 5 \times 10^4 \text{ cm}^{-3}$  and peak diameter of  $\sim 5$  nm indicating fresh nucleation events (Figure 5a). The default WRF-Chem simulations also capture this large source of small particles due to nucleation (Figure 5c). Observations indicate that the nucleated particles grow to  $\sim 50$  nm by late afternoon that is, 16:30 CDT. However, the noAnthrop ELVOC simulation (Figure 5e, that excludes anthropogenic ELVOCs) predicts a much broader final size distribution (larger spread close to 17 CDT in particle number) and most particles are smaller than the simulated peak diameter of  $\sim 20$  nm that is inconsistent with the observations. Thus, the difference between default and noAnthrop ELVOC simulations (middle panels vs. bottom panels in Figure 5) indicates that anthropogenic ELVOCs are critical for growing the nucleated particles by overcoming the Kelvin



**Figure 5.** Observed (top panels) and WRF-Chem simulated (middle and bottom panels) time evolution of aerosol size distributions showing new particle formation and growth at the SGP site on 28 April 2016 (left panels) and 14 May 2016 (right panels). Middle panel (c and d) depict simulations for the default case that includes ELVOCs from all sources (anthropogenic, biogenic, and biomass burning), whereas the bottom panel (e and f) shows a sensitivity simulation that includes ELVOCs from biogenic and biomass burning but excludes anthropogenic ELVOCs. The solid horizontal black lines indicate peak diameter of the size distribution at any given time, whereas the dotted horizontal black line indicates final diameters.

barrier and increasing their survival against coagulation. As with 28 April, the no Anthrop ELVOC simulation on 14 May fails to grow the nucleated particles and most particles stay below 5 nm by 18 CDT (Figure 5f), which is inconsistent with observations that show particles growing to ~30 nm (Figure 5b). The default simulation that includes Anthropogenic ELVOCs uniquely explain the observed late afternoon peak and shape of particle size distributions at the SGP site (Figure 5d). In comparison to anthropogenic ELVOCs, the role of biomass burning ELVOCs at the SGP site during these days was minor. As shown in Figure S10 in Supporting Information S1, removing biomass burning ELVOCs (no BiomBurn ELVOC) did not affect the growth and evolution of particle size distribution as much as the no Anthrop ELVOC simulation.

For visual clarity of the particle size distribution statistics, Figure S11 in Supporting Information S1 compares modeled and observed size distributions for the default and no anthropogenic ELVOC simulations during discrete times of ~10, 12, 15, and 17 CDT corresponding to Figure 5. On both 28 April and 14 May, Figure S11 in Supporting Information S1 shows that the observed peak in the nucleation mode (black dots) occurs around 3 nm in the mornings (10–11 CDT), whereas the modeled nucleation mode peaks are below 2 nm. Note that the observations only go down to 3 nm diameter particle sizes; therefore, it is not possible to evaluate the model predicted particle size distributions below 3 nm particle diameter. At around 12 CDT, the modeled nucleation mode grows and approaches the observed growing mode of ~20 nm diameter. The default simulation (blue, Figure S11 in Supporting Information S1) approaches the growing mode faster than the simulation without anthropogenic ELVOCs (no anthrop ELVOC, red). At ~15–16 CDT, the default model (blue, Figure S11 in Supporting Information S1) predicts that the nucleation mode has grown to ~20 nm diameter on 28 April, whereas the observed mode is at ~30 nm diameter and the number concentration of particles with sizes <2 nm

diameter has dropped substantially in both default model and observations (compare 15 CDT vs. 10 CDT). In sharp contrast, the simulation without anthropogenic ELVOCs (red, Figure S11 in Supporting Information S1) shows an order of magnitude higher particle number concentrations at sizes  $<2$  nm diameter compared to the observations and the default model. Due to the lack of anthropogenic ELVOCs, around 50% of the particles exist in 3–10 nm size range at 15 CDT, in comparison to 8% in observations and 4% in the default model. Observations (black dots in Figure S11 in Supporting Information S1) show that on 28 April,  $\sim 85\%$  of the total particle number concentrations are in the size range 10–50 nm, while a much smaller fraction (50%) exist in this size range within the no anthrop ELVOC simulation. In the default model,  $\sim 90\%$  of the particles have grown to 10–50 nm size range consistent with observations. The above statistics and Figure 5 and Figure S11 in Supporting Information S1 clearly show that the simulation without anthropogenic ELVOCs substantially overestimates number concentrations of particles  $<10$  nm diameter and underestimates particles in the 10–50 nm diameter range compared to observations. Including anthropogenic ELVOC formation in the default model causes the model to agree much better with the evolution of particle size distributions on both 28 April and 14 May.

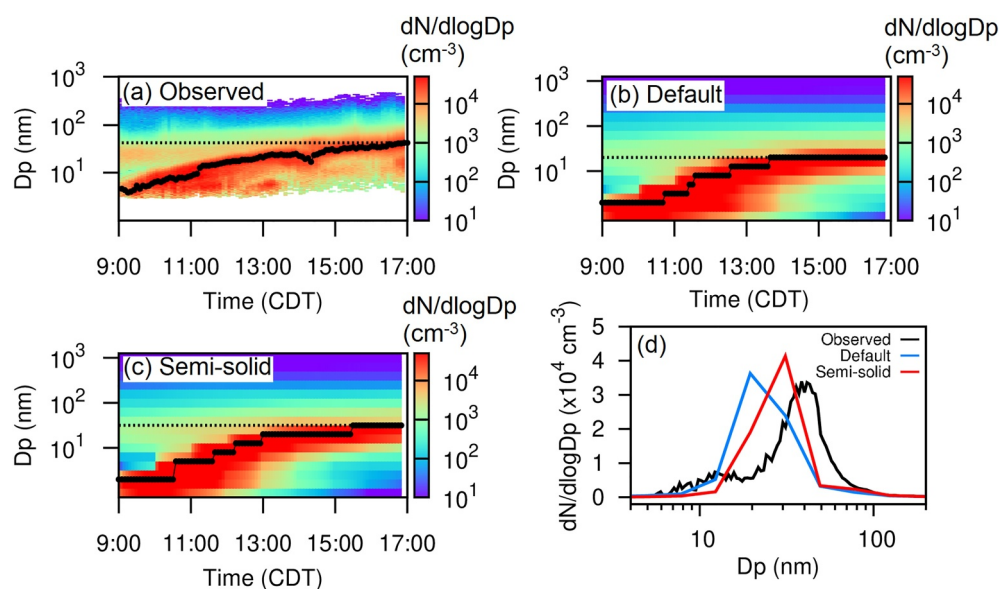
Consistent with the above analyses at the fixed SGP site, additional analyses of Lagrangian forward and backward particle trajectories from the SGP site using the HYSPLIT model show how the air parcel encountered large nucleation events around 9 CDT (morning), and subsequently, the nucleated particles grew as the air parcel moved to encounter the SGP site at 14 CDT (afternoon), as shown in Figure S12 and S13 in Supporting Information S1, and discussed in further detail in the Supplementary Information.

### 3.4. Observed and Simulated Particle Size Distributions Onboard the G-1 Aircraft

Similar to NPF and growth observed near the ground at SGP, aircraft measurements provide useful insights about particle growth at higher altitudes. As an example, Figure S14 in Supporting Information S1 compares observed and simulated particle size distributions onboard the G-1 aircraft on 28 April. Similar to the ground-based observations, WRF-Chem without any additional ELVOCs from anthropogenic and biomass burning sources (orange, no Anth/BB ELVOC that still includes monoterpene ELVOCs/ULVOCs) fails to grow the particles to the observed sizes (red). Adding ELVOCs from both anthropogenic and biomass burning sources (blue, default) results in more growth that is closer to observations, further highlighting the role of ELVOCs from anthropogenic VOCs in growth. Including anthropogenic ELVOCs but removing biomass burning ELVOCs (noBiomELVOC, green) is closer to the default simulation showing smaller impacts of biomass burning ELVOCs on simulated particle growth.

### 3.5. Effects of Particle Phase State on Simulated Growth

The phase state of SOA governs the gas-particle equilibrium timescales due to changes in the bulk diffusion and mass transfer of semi-volatile organic gases within particles (Zaveri et al., 2014, 2022). Liquid-like particles attain equilibrium almost instantaneously, with condensing organic gases dispersing rapidly throughout the particle's bulk. In contrast, semisolid/solid particles take much longer to attain equilibrium depending on particle size. Bulk diffusion timescales increase with an increase in the square of the particle diameter, implying that semi-volatile organics condensing to semisolid particles can grow smaller particles faster than they grow larger ones (Zaveri et al., 2014). Consequently, a semisolid phase state of particles would facilitate more rapid growth of nucleated particles compared to liquid-like particles (Zaveri et al., 2022). As SOA particles age in the atmosphere, their phase state might change from liquid-like to semisolid phase, especially for particles that have grown to accumulation mode range ( $>100$  nm diameter) and contain significant oligomers in the particle phase (Shrivastava et al., 2017; Zaveri et al., 2022). Due to lack of measurements of particle-phase state during HI-SCALE, all the simulations presented previously (default, no Anthrop ELVOC, no BiomBurn ELVOC, no ELVOC) adopted a volatility- and relative humidity (RH)- dependent parameterization of viscosity of SOA within WRF-Chem (Rasool et al., 2021), and corresponding predicted bulk particle diffusivities ranged from  $10^{-11}$  to  $10^{-13}$   $\text{cm}^2 \text{s}^{-1}$  near the surface at SGP. Although these diffusivities are in the semisolid range, lower bulk diffusivities  $<10^{-15}$   $\text{cm}^2 \text{s}^{-1}$  are needed to significantly affect gas-particle partitioning kinetics of semi-volatile organics (Zaveri et al., 2014). Note that the viscosity parameterization in WRF-Chem does not account for particle-phase aging and oligomer formation that is expected to reduce particle volatility and increase viscosity (reduce bulk diffusivity) (Shrivastava et al., 2015, 2017). To investigate the effect of stronger bulk diffusion limitations within the semisolid phase state of SOA, we conduct a sensitivity run for the default simulation assuming that SOA particles with diameter  $>100$  nm (that have experienced growth and aging in the atmosphere)

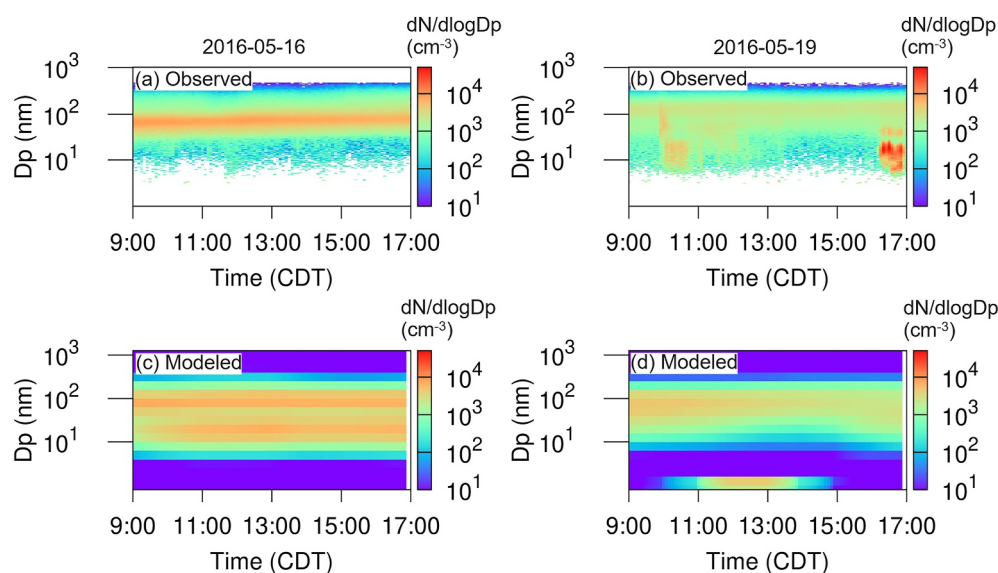


**Figure 6.** WRF-Chem simulated time evolution of aerosol size distributions showing new particle formation and growth at the SGP site on 28 April 2016. (a) Observed (b) default simulation with a predicted bulk diffusivity ranging between  $10^{-11}$  and  $10^{-15}$   $\text{cm}^2 \text{s}^{-1}$  for all particle sizes (c) Sensitivity simulation that assumes a lower bulk diffusivity of  $10^{-15}$   $\text{cm}^2 \text{s}^{-1}$  for secondary organic aerosol particles with diameter  $>100$  nm and  $10^{-10}$   $\text{cm}^2 \text{s}^{-1}$  for particles  $<50$  nm, as described in the text (d) final particle size distributions at 17 CDT. The solid horizontal black lines in (a)–(c) indicate peak diameter of the size distribution at any given time, whereas the dotted horizontal black line indicates final diameters.

are semi-solid with a bulk diffusivity of  $10^{-15}$   $\text{cm}^2 \text{s}^{-1}$ , whereas smaller particles ( $<50$  nm) are assumed to have a relatively larger bulk diffusivity of  $10^{-10}$   $\text{cm}^2 \text{s}^{-1}$ , following Zaveri et al. (2022). As described in Zaveri et al. (2022), SOA particles  $>100$  nm represent aged accumulation mode particles that are expected to have higher oligomer content (higher viscosities and lower bulk diffusivities) than relatively fresh smaller SOA particles. Figure 6 shows this assumption of lower bulk diffusivity of  $10^{-15}$   $\text{cm}^2 \text{s}^{-1}$  for particles with diameter  $>100$  nm (Figure 6c) predicts faster growth compared to the default simulation (Figure 6b) and agrees better with observations (Figure 6a). The final size distribution at 17 CDT (Figure 6d) shows that compared with the observed peak diameter of  $\sim 50$  nm (black), the default simulation (blue) grows to a peak diameter of 20 nm while the strongly diffusion-limited semi-solid assumption grows to a peak diameter of  $\sim 35$  nm. Above analysis implies that larger particles at the SGP site were likely highly aged and their low bulk diffusivity diminished their role as sinks for low volatility organic gases, which increased the availability of low volatility organic vapors for faster growth of smaller particles from nucleated clusters compared to default model predictions.

### 3.6. Simulations of Non-NPF Days

In addition to NPF event days, it is useful to assess the performance of the model in simulating non-NPF event days. 16 and 19 May were identified as non-NPF event days from the analyses of observed particle size distributions at the SGP site (O'Donnell et al., 2023). We conducted WRF-Chem simulations to assess whether the model could be used to reproduce the absence of NPF as observed at the SGP site, and whether WRF-Chem simulations could be used to understand the reasons for the absence of NPF on these days compared to the NPF days (28 April and 14 May 2016 as discussed above). Figures 7a and 7b (top panels) show the SMPS measured particle size distributions over the SGP surface site during the daytime for 16 and 19 May, which were characterized by the absence of clear NPF and growth events. WRF-Chem simulations (in Figure 7c) show absence of nucleation and growth on 16 May in agreement with observations (Figure 7a). On 19 May, WRF-Chem predicts nucleation between 11 and 15 CDT; however, these nucleation rates are much lower peaking at  $\sim 1$   $\text{cm}^{-3} \text{s}^{-1}$  compared to peak nucleation rates of  $10$ – $100$   $\text{cm}^{-3} \text{s}^{-1}$  simulated on the NPF event days. WRF-Chem simulations indicate that the nucleated particles on 19 May (with sizes less than 3 nm) did not grow further due to cloudy skies causing lower oxidants (OH radicals) resulting in substantially lower amounts of



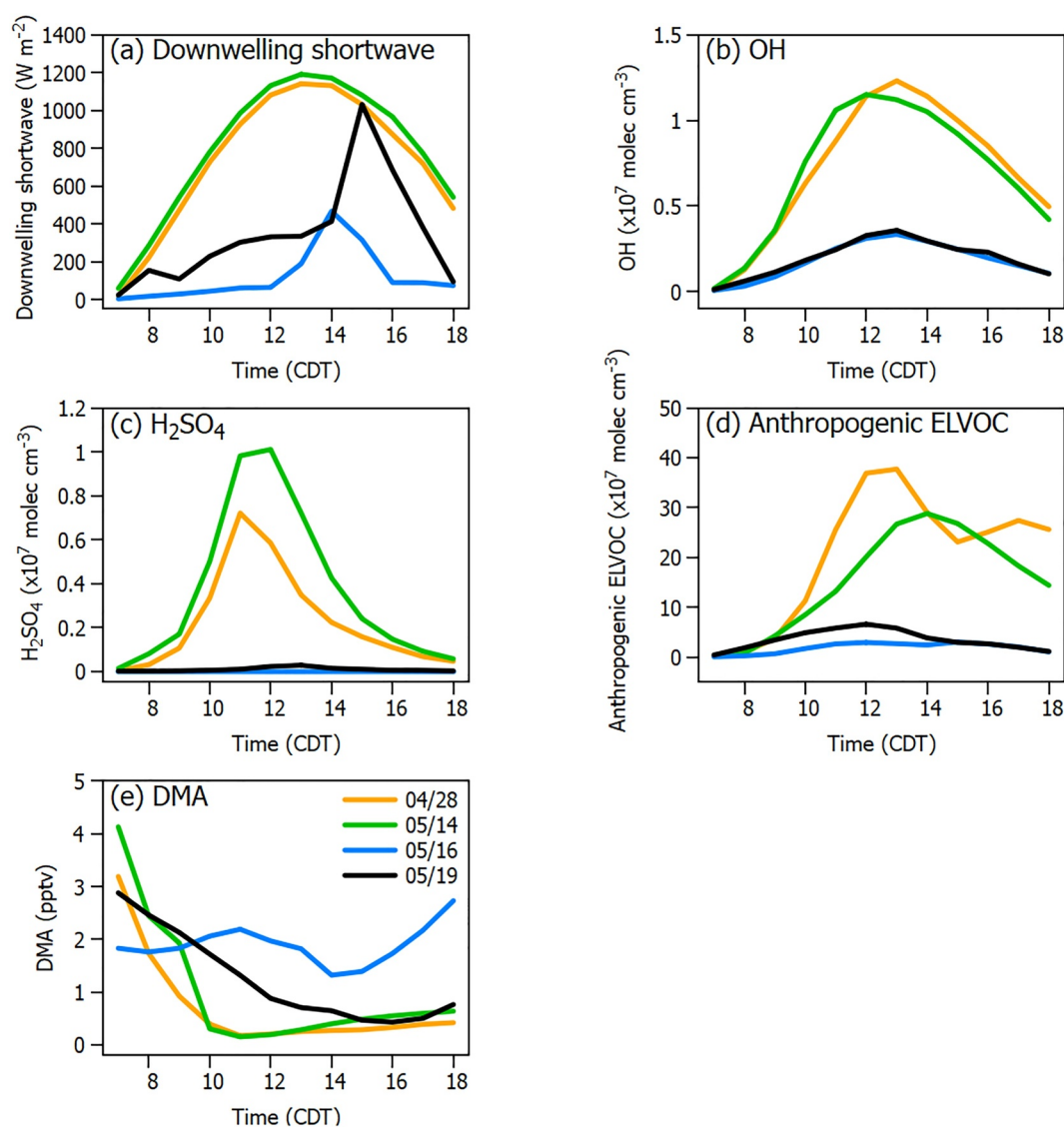
**Figure 7.** Observed (top panels) and WRF-Chem simulated (bottom panels with semi-solid formulation) time evolution of aerosol size distributions showing the absence of new particle formation and growth at the SGP site on the two non-NPF days of 16 May 2016 (left panels) and 19 May 2016 (right panels).

ELVOCs formed and lower  $\text{H}_2\text{SO}_4$  gas concentrations compared to NPF event days of 28 April and 14 May as shown in Figures 8b and 8d as well as discussed below.

We note that while the NPF event days 28 April and 14 May were mostly sunny, the non-NPF days (16 and 19 May) were overcast with clouds (see Figure S15 in Supporting Information S1 that compares MODIS satellite images during 28 April and 16 May). Figure 8a shows that due to cloudy skies, the downwelling shortwave radiation reaching the surface SGP site during the daytime was substantially lower on the non-NPF event days (blue and black lines in Figure 8a) compared to the NPF event days (orange and green lines in Figure 8a). WRF-Chem simulated differences in downwelling shortwave radiation between NPF and non-NPF days are consistent with measurements of downwelling shortwave radiation at the SGP surface site, as indicated in Figure S16 in Supporting Information S1. Due to reduced photochemical activity, OH radical concentrations are reduced by  $\sim$  factor of 4 as shown in Figure 8b at SGP surface site on non-NPF days (blue and black lines) compared with the NPF days (orange and green lines) and the regional OH maps Figure S6a in Supporting Information S1 (28 April) versus Figure S6d in Supporting Information S1 (16 May). Due to reduced OH radical concentrations on cloudy days, the WRF-Chem simulated concentrations of anthropogenic ELVOCs and  $\text{H}_2\text{SO}_4$  gases are at least an order of magnitude lower on non-NPF days (blue and black lines in Figures 8c and 8d) compared to the NPF event days (orange and green lines in Figures 8c and 8d). On our NPF event days of 28 April and 14 May, WRF-Chem simulated  $\text{H}_2\text{SO}_4$  gas-phase concentrations are  $\sim 2 \times 10^6$  molecule  $\text{cm}^{-3}$  as shown in Figure 8c at the beginning of the nucleation event  $\sim 10$  CDT, whereas anthropogenic ELVOC gases (Figure 8d) are  $\sim 10^8$  molecule  $\text{cm}^{-3}$ . Our WRF-Chem simulated  $\text{H}_2\text{SO}_4$  gas-phase concentrations of  $2 \times 10^6$  molecule  $\text{cm}^{-3}$  are within the range of measured  $\text{H}_2\text{SO}_4$  concentrations using the CIMS instrument during nucleation events at the SGP site in a different year (spring 2013) as reported in Table 1 of Hodshire et al. (2016). As discussed above,  $\text{H}_2\text{SO}_4$  is a key species needed to nucleate clusters, while both  $\text{H}_2\text{SO}_4$  and ELVOCs are important for the growth of these clusters to ultrafine particle sizes, and their low concentrations explain the absence of NPF on the cloudy days, shown in Figure 7.

WRF-Chem simulated DMA gas concentrations peak at 2–4 pptv in the early morning (before 8 CDT) but then drop substantially approaching zero at  $\sim 10$  CDT (Figure 8e, orange and green lines) at the beginning of nucleation on 28 April and 14 May since they are taken up by particles during nucleation and also react with OH radicals. Recently, Katz et al. (2023) found that C3 amines were more abundant than C2 amines (that likely include DMA) during the summer in the vicinity of the SGP site, but we could not find any quantitative values reported for evaluating our model predictions of gas-phase DMA in their study. In addition, the Katz et al. (2023) measurements were conducted in the summer while our modeling study is focused on the spring season. Due to





**Figure 8.** WRF-Chem simulations comparing key quantities responsible for particle nucleation during new particle formation (NPF) events (28 April and 14 May) and non-NPF days (16 and 19 May) at the SGP surface site during the daytime showing (a) Downwelling shortwave radiation ( $\text{W m}^{-2}$ ) (b) Gas-phase OH radical concentrations ( $\text{molecule cm}^{-3}$ ) (c)  $\text{H}_2\text{SO}_4$  gas concentrations ( $\text{molecule cm}^{-3}$ ) (d) Anthropogenic ELVOC gas concentrations ( $\text{molecule cm}^{-3}$ ) (e) DMA gas concentrations (pptv).

seasonal variations in biogenic emissions and photochemistry, our simulations cannot be evaluated with measurements reported by Katz et al. (2023).

Measurements at the SGP site during the spring in 2013 in Hodshire et al. (2016) reported that sum of methylamine, DMA, and trimethylamines ranged 10–100 pptv. Our simulated DMA concentrations (Figure 8e) are lower than the sum of amines reported in Hodshire et al. (2016); however, since DMA alone was not reported, it is difficult to evaluate our simulated DMA with Hodshire et al. (2016). In addition, the amine measurements made in 2013 with their ambient pressure proton transfer mass spectrometer (AmPMS) instrument might have higher uncertainties due to its lower mass resolution compared to more advanced higher resolution mass spectrometers that are currently available (Katz et al., 2023; Olin et al., 2022). Therefore, deploying these higher resolution mass spectrometers is critical for quantifying how amines contribute to nucleation at SGP and other locations. Simulated DMA concentrations are higher on the cloudy non-NPF days compared to the NPF days (Figure 8e), since reduced OH concentrations (Figure 8b) reduce the photochemical losses of DMA on the cloudy days.

Contrasting NPF and non-NPF days, we clearly find the important role of clouds in modulating photochemistry and NPF processes in the atmosphere.

### 3.7. Model Sensitivity to DMA Emissions Ratio at SGP

All the simulations in this work used an assumed ratio of DMA to  $\text{NH}_3$  of 0.0015, which represents a lower bound emissions ratio corresponding to agricultural regions as documented in Y. Li et al. (2023), while an upper bound ratio of 0.007 corresponds to chemical-industrial sources and is 5 times higher than our assumed ratio (Y. Li et al., 2023). To investigate the sensitivity of WRF-Chem simulated NPF to DMA emissions, we conducted a simulation with the upper bound ratio of DMA to  $\text{NH}_3$  of 0.007 for 28 April 2016, as shown in Figure S17 in Supporting Information S1. Compared to the default WRF-Chem simulation with lower bound DMA emissions used in this study (Figure S17b in Supporting Information S1), using an upper bound of DMA emissions (Figure S17c in Supporting Information S1) increases particles smaller than 10 nm even at the later stages of particle growth (at around 15 CDT). However, measurements (Figure S15a in Supporting Information S1) do not show evidence of this peak in sub 10 nm particles at this later afternoon time, suggesting the default simulations with the lower bound of DMA to  $\text{NH}_3$  of 0.0015 representing agricultural regions are closer to observations. Since SGP region is surrounded by agricultural regions, we expect our assumed ratio for agricultural regions of 0.0015 to be more applicable. However, we note that changing the DMA emissions ratio does not affect the main results and conclusions of this work regarding the role of DMA, anthropogenic ELVOCs and  $\text{H}_2\text{SO}_4$  on NPF and growth in the vicinity of the SGP site.

### 3.8. Lack of NPF at the BNF Site in SE USA During These Days

In contrast to clear NPF events observed at the SGP site, WRF-Chem predicts no clear NPF events on 28 April and 14 May at BNF site as shows in Figure S18 in Supporting Information S1. This lack of NPF at BNF site on the same days when NPF was detected at the SGP site is due to  $\sim 2$  orders of magnitude lower simulated  $\text{H}_2\text{SO}_4$  gas concentrations (peak  $\text{H}_2\text{SO}_4$  gas concentrations  $< 1 \times 10^5$  during the afternoon on 14 May and  $4 \times 10^5$  molecule  $\text{cm}^{-3}$  on 28 April, Figure S19b in Supporting Information S1) compared to peak  $\text{H}_2\text{SO}_4$  gas concentrations  $\sim 10^7$  molecule  $\text{cm}^{-3}$  simulated at the SGP site on these days (Figure 8c). Note that in the morning (10 CDT), at the onset of nucleation at SGP, simulated  $\text{H}_2\text{SO}_4$  gas concentrations are  $\sim 2 \times 10^6$  molecule  $\text{cm}^{-3}$ , whereas  $\text{H}_2\text{SO}_4$  gas concentrations at BNF are orders of magnitude lower (even lower than their peak afternoon values at BNF).

Although BNF measurements are not yet available, previous measurements in an isoprene-influenced mixed deciduous forest site (Brent, Alabama) during the southern oxidant and aerosol study (SOAS) 2013 field campaign in the summertime provide additional insights, as described in Lee et al. (2016). Their observations showed that nucleation rates were proportional to  $\text{H}_2\text{SO}_4$  gas concentrations and sub-2 nm diameter particles were detected when  $\text{H}_2\text{SO}_4$  concentrations exceeded  $10^5$  molecules  $\text{cm}^{-3}$ . However, the freshly nucleated 2 nm particles rarely grew to larger sizes in the forest. It was suggested that isoprene suppresses NPF within the forested site and this suppression was likely due to chemical cross-reactions of isoprene with sulfuric acid, since  $\text{H}_2\text{SO}_4$  concentrations at the site were similar to those observed within boreal forests in Finland where NPF occurs frequently. Recently, Schervish et al. (2024) investigated the  $\text{RO}_2$  cross-reactions between monoterpene and isoprene oxidation products by combining observations from the CLOUD experiments at CERN and the radical volatility basis set (radical-VBS). They found that isoprene interferes with covalently bonded  $\text{C}_{20}$  dimers formed in the pure monoterpene system, consequently reducing formation rate of ultralow volatility organics (ULVOCs) and associated nucleation rates. However, the presence of isoprene has less of an effect on particle growth rates. Currently, our WRF-Chem simulations do not include the chemical cross-reactions between isoprene and other HOMs within our R2D-VBS, and we do not consider the reduction of nucleation rates due to cross-reactions between isoprene and monoterpene  $\text{RO}_2$ . Including these reactions might further reduce nucleation rates with less of an influence on particle growth rates at BNF. Despite the potential model overestimation of nucleation rates due to lack of isoprene suppression of ULVOCs, WRF-Chem predicts no clear NPF events on 28 April and 14 May at BNF site as shows in Figure S18 in Supporting Information S1. Compared to SGP, the BNF site has two orders-of-magnitude lower  $\text{H}_2\text{SO}_4$  and almost an order of magnitude higher CS in the early mornings (at the onset of nucleation), which explain the absence of clear NPF and growth at BNF during our two simulated days. However, further investigation over other days including the summertime are needed to assess the lack of NPF reported over SE USA in previous studies. We also note that even at the SGP site during HI-SCALE 2016, nucleation events were more frequent during spring compared to summertime. While the SOAS 2013 field

campaign was during summer, detailed gas- and particle-phase measurements are needed in the spring in SE USA to further assess the mechanisms governing particle growth and NPF.

#### 4. Conclusions

The SGP site in central Oklahoma has been a region of great interest for studying aerosol-cloud interactions since it experiences regionally transported air masses influenced by urban, grassland, and cropland source regions. In addition, the presence of long term and historic measurements and the recent HI-SCALE field measurements (Fast et al., 2019) provide a good data set for evaluating aerosol processes represented in detailed regional models. However, large uncertainties prevail in our understanding of processes governing NPF and their growth to CCN sizes in this region. During the springtime, when biogenic activity and SOA formation are low, NPF events have frequently been observed at SGP. Here, we use a detailed regional model to investigate the processes governing NPF and SOA formation in this region.

WRF-Chem simulations indicate that SOA formed at SGP was strongly influenced by anthropogenic sources during the two NPF event springtime days with northerly winds consistent with a previous 1-D column modeling study over SGP (O'Donnell et al., 2023). We show that large particle nucleation rates at SGP can be attributed primarily to DMA and H<sub>2</sub>SO<sub>4</sub>. However, we did not consider the likely synergistic role of NH<sub>3</sub> in the nucleation rates involving DMA and H<sub>2</sub>SO<sub>4</sub>, although NH<sub>3</sub> might reduce the dependence of nucleation and particle number on DMA for a given H<sub>2</sub>SO<sub>4</sub> concentration (DePalma et al., 2012; Glasoe et al., 2015). Field measurements in urban Beijing have shown that clusters were initially formed by amine and H<sub>2</sub>SO<sub>4</sub> molecules, but as cluster size increases, amine fractions in ion acid-base clusters decrease while NH<sub>3</sub> fractions in these clusters increase (Yin et al., 2021). Similar field measurements are needed to understand the likely synergistic role of NH<sub>3</sub> in nucleation rates involving DMA and H<sub>2</sub>SO<sub>4</sub> at SGP, BNF, and other locations and inform WRF-Chem simulations in the future. Using WRF-Chem, we also simulate two non-NPF days determined from observed particle size distributions at SGP and show that overcast low-level clouds that reduce photochemical activity near the surface during these days are primarily responsible for the absence of NPF. Comparing simulations of both NPF and non-NPF event days in WRF-Chem, we highlight the role of clouds in decreasing NPF and ultrafine particle concentrations at the SGP site. Although SOA concentrations at SGP are predicted to be much lower than the BNF site in the southeastern U.S., which is strongly influenced by biogenic SOA formation, the smaller CS at SGP promotes the survival probability of nucleated molecular clusters and their growth to CCN sizes. At the BNF site, H<sub>2</sub>SO<sub>4</sub> concentrations are an order of magnitude lower than SGP resulting in 1–2 orders of magnitude smaller nucleation rates than the SGP site. In addition, higher summertime temperatures at BNF compared to the springtime at SGP might also partly explain the lower observed NPF at BNF compared to SGP, since nucleation and growth rates are temperature dependent. Our simulations show that at SGP, anthropogenic ELVOCs play a critical role in explaining the observed growth and evolution of the particle size distribution from early morning to late afternoon during our two simulated NPF event days in the springtime.

CCN number at any given location depends on the history of nucleation and SOA formation mechanisms that air parcels experience as they arrive at the location. In forested regions around the world, biogenic emissions have been reported to be key drivers of CCN and aerosol-cloud interactions (Petäjä et al., 2022). However, at locations such as SGP that are far away from forests and during times of low biogenic influence (e.g., in the springtime during northerly winds at SGP), our work implies that DMA and H<sub>2</sub>SO<sub>4</sub> could be key nucleation drivers especially in clear sky conditions as shown for the two NPF events simulated in this study, whereas the anthropogenic low volatility organics formed by the atmospheric oxidation of aromatic VOCs could maintain sufficient particle growth to CCN sizes that interact with clouds and radiation in the atmosphere. Given their critical role in nucleation as suggested by our WRF-Chem simulations, it would be important to obtain continuous measurements of amines, H<sub>2</sub>SO<sub>4</sub>, NH<sub>3</sub>, and neutral and naturally charged ion clusters with recent advanced instruments that have high sensitivity and mass resolution for these species at SGP and BNF sites during the springtime. Although measurements of anthropogenic ELVOC yields in the gas-phase are lacking, we conducted sensitivity studies using advanced NPF and SOA modules within WRF-Chem to derive important insights about ELVOCs needed for explaining the observed particle growth at the SGP site. Comparing WRF-Chem simulations of observed NPF and non-NPF days at SGP and the predicted lack of NPF at BNF site during our simulated days, we find that H<sub>2</sub>SO<sub>4</sub> concentrations (modulated by clouds and photochemical activity) and CS are key factors that could explain the presence (or absence) of NPF in our simulations. Future co-located measurements of gas-phase ELVOC yields from anthropogenic precursors with particle size distributions (down to the smallest particle

diameters <2 nm) and chemical composition of ultrafine particles (with diameters <30 nm) are needed for improving NPF processes in models for more accurate predictions of CCN and getting the right answers for the right reasons.

### Data Availability Statement

All data analyzed during the current study are included in this published article and its supplementary information. Measured data during the HI-SCALE 2016 field campaign are publicly available on the Atmospheric Radiation Measurement (ARM) website: <https://www.arm.gov/research/campaigns/sgp2016hiscale>. The WRF4.2 code used in our Manuscript is publicly available at [https://www2.mmm.ucar.edu/wrf/users/download/get\\_source.html](https://www2.mmm.ucar.edu/wrf/users/download/get_source.html) with specific modifications as documented at <https://www.abacas-dss.com/abacas/abacas/CMANModel.aspx>. Figures in the main text and supplementary information were made with Gnuplot version 5.2 available at <http://sourceforge.net/projects/gnuplot> and the near ncl scripts for WRF-Chem available at <https://www.ncl.ucar.edu/>.

### Acknowledgments

This research was supported by the U.S. Department of Energy (DOE) Office of Science, Office of Biological and Environmental Research (BER) through the Early Career Research Program and DOE BER's Atmospheric System Research (ASR) program. JRP and SEO acknowledge the support from the Atmospheric System Research (ASR) program, part of the US Department of Energy's Office of Biological and Environmental Research within the Office of Science, under Grants DE-SC0019000, DE-SC0021208. Funding for data collection onboard the G-1 aircraft and at the ground sites was provided by the Atmospheric Radiation Measurement (ARM) Climate Research Facility, a DOE user facility sponsored by BER. The Pacific Northwest National Laboratory (PNNL) is operated for DOE by Battelle Memorial Institute under contract DE-AC06-76RL01830. Computational resources for the simulations were provided by EMSL (a DOE Office of Science User Facility sponsored by the Office of Biological and Environmental Research located at PNNL) and National Energy Research Scientific Computing Center (NERSC), which is a US DOE Office of Science User Facility operated under contract no. DE-AC02-05CH11231. The authors gratefully acknowledge the NOAA Air Resources Laboratory (ARL) for the provision of the HYSPLIT transport and dispersion model and/or READY website (<https://www.ready.noaa.gov>) used in this publication. B. Zhao acknowledges the funding of the Samsung Advanced Institute of Technology. The views expressed in this article are those of the author(s) and do not necessarily represent the views or the policies of the U. S. Environmental Protection Agency. We thank Coty Jen for helpful discussions about measurements of amines.

### References

Akherati, A., He, Y., Coggon, M. M., Koss, A. R., Hodshire, A. L., Sekimoto, K., et al. (2020). Oxygenated aromatic compounds are important precursors of secondary organic aerosol in biomass-burning emissions. *Environmental Science & Technology*, *54*(14), 8568–8579. <https://doi.org/10.1021/acs.est.0c01345>

Bianchi, F., Kurten, T., Riva, M., Mohr, C., Rissanen, M. P., Roldin, P., et al. (2019). Highly oxygenated organic molecules (HOM) from gas-phase autoxidation involving peroxy radicals: A key contributor to atmospheric aerosol. *Chemical Reviews*, *119*(6), 3472–3509. <https://doi.org/10.1021/acs.chemrev.8b00395>

Brege, M. A., China, S., Schum, S., Zelenyuk, A., & Mazzoleni, L. R. (2021). Extreme molecular complexity resulting in a continuum of carbonaceous species in biomass burning tar balls from wildfire smoke. *ACS Earth and Space Chemistry*, *5*(10), 2729–2739. <https://doi.org/10.1021/acsearthspacechem.1c00141>

Chen, Y., Takeuchi, M., Nah, T., Xu, L., Canagaratna, M. R., Stark, H., et al. (2020). Chemical characterization of secondary organic aerosol at a rural site in the southeastern US: Insights from simultaneous high-resolution time-of-flight aerosol mass spectrometer (HR-ToF-AMS) and FIGAERO chemical ionization mass spectrometer (CIMS) measurements. *Atmospheric Chemistry and Physics*, *20*(14), 8421–8440. <https://doi.org/10.5194/acp-20-8421-2020>

Cheng, X., Chen, Q., Jie Li, Y., Zheng, Y., Liao, K., & Huang, G. (2021). Highly oxygenated organic molecules produced by the oxidation of benzene and toluene in a wide range of OH exposure and NO<sub>x</sub> conditions. *Atmospheric Chemistry and Physics*, *21*(15), 12005–12019. <https://doi.org/10.5194/acp-21-12005-2021>

Cheng, X., Li, Y. J., Zheng, Y., Liao, K., Koenig, T. K., Ge, Y., et al. (2024). Oxygenated organic molecules produced by low-NO<sub>x</sub> photooxidation of aromatic compounds: Contributions to secondary organic aerosol and steric hindrance. *Atmospheric Chemistry and Physics*, *24*(4), 2099–2112. <https://doi.org/10.5194/acp-24-2099-2024>

Darmenov, A. S., & da Silva, A. (2015). The Quick Fire Emissions Dataset (QFED): Documentation of versions 2.1, 2.2 and 2.4. In *Technical Report Series on Global Modeling and Data Assimilation*.

DePalma, J. W., Bzdek, B. R., Doren, D. J., & Johnston, M. V. (2012). Structure and energetics of nanometer size clusters of sulfuric acid with ammonia and dimethylamine. *The Journal of Physical Chemistry A*, *116*(3), 1030–1040. <https://doi.org/10.1021/jp210127w>

Dowell, D. C., Alexander, C. R., James, E. P., Weygandt, S. S., Benjamin, S. G., Manikin, G. S., et al. (2022). The High-Resolution Rapid Refresh (HRRR): An hourly updating convection-allowing forecast model. Part I: Motivation and system description. *Weather and Forecasting*, *37*(8), 1371–1395. <https://doi.org/10.1175/waf-d-21-0151.1>

Dunne, E. M., Gordon, H., Kürten, A., Almeida, J., Duplissy, J., Williamson, C., et al. (2016). Global atmospheric particle formation from CERN CLOUD measurements. *Science*, *354*(6316), 1119–1124. <https://doi.org/10.1126/science.1264949>

Ehn, M., Berndt, T., Wildt, J., & Mentel, T. (2017). Highly oxygenated molecules from atmospheric autoxidation of hydrocarbons: A prominent challenge for chemical kinetics studies. *International Journal of Chemical Kinetics*, *49*(11), 821–831. <https://doi.org/10.1002/kin.21130>

Ehn, M., Thornton, J. A., Kleist, E., Sipila, M., Junninen, H., Pullinen, I., et al. (2014). A large source of low-volatility secondary organic aerosol. *Nature*, *506*(7489), 476–479. <https://doi.org/10.1038/nature13032>

Emmons, L. K., Schwantes, R. H., Orlando, J. J., Tyndall, G., Kinnison, D., Lamarque, J.-F., et al. (2020). The Chemistry Mechanism in the Community Earth System Model Version 2 (CESM2). *Journal of Advances in Modeling Earth Systems*, *12*(4), e2019MS001882. <https://doi.org/10.1029/2019MS001882>

Fast, J. D., Berg, L. K., Alexander, L., Bell, D., D'Ambro, E., Hubbe, J., et al. (2019). Overview of the HI-SCALE field campaign: A new perspective on shallow convective clouds. *Bulletin of the American Meteorological Society*, *100*(5), 821–840. <https://doi.org/10.1175/bams-d-18-0030.1>

Fast, J. D., Gustafson, W. I., Easter, R. C., Zaveri, R. A., Barnard, J. C., Chapman, E. G., et al. (2006). Evolution of ozone, particulates, and aerosol direct radiative forcing in the vicinity of Houston using a fully coupled meteorology-chemistry-aerosol model. *Journal of Geophysical Research*, *111*(D21), D21305. <https://doi.org/10.1029/2005jd006721>

Foley, K. M., Pouliot, G. A., Eyth, A., Aldridge, M. F., Allen, C., Appel, K. W., et al. (2023). 2002–2017 anthropogenic emissions data for air quality modeling over the United States. *Data in Brief*, *47*, 109022. <https://doi.org/10.1016/j.dib.2023.109022>

Garmash, O., Rissanen, M. P., Pullinen, I., Schmitt, S., Kausiala, O., Tillmann, R., et al. (2020). Multi-generation OH oxidation as a source for highly oxygenated organic molecules from aromatics. *Atmospheric Chemistry and Physics*, *20*(1), 515–537. <https://doi.org/10.5194/acp-20-515-2020>

Ge, X., Wexler, A. S., & Clegg, S. L. (2011). Atmospheric amines – Part I. A review. *Atmospheric Environment*, *45*(3), 524–546. <https://doi.org/10.1016/j.atmosenv.2010.10.012>

Glasoe, W. A., Volz, K., Panta, B., Freshour, N., Bachman, R., Hanson, D. R., et al. (2015). Sulfuric acid nucleation: An experimental study of the effect of seven bases. *Journal of Geophysical Research: Atmospheres*, *120*(5), 1933–1950. <https://doi.org/10.1002/2014JD022730>

Grell, G. A., Peckham, S. E., Schmitz, R., McKeen, S. A., Frost, G., Skamarock, W. C., & Eder, B. (2005). Fully coupled “online” chemistry within the WRF model. *Atmospheric Environment*, *39*(37), 6957–6975. <https://doi.org/10.1016/j.atmosenv.2005.04.027>

- Guo, Y., Yan, C., Liu, Y., Qiao, X., Zheng, F., Zhang, Y., et al. (2022). Seasonal variation in oxygenated organic molecules in urban Beijing and their contribution to secondary organic aerosol. *Atmospheric Chemistry and Physics*, 22(15), 10077–10097. <https://doi.org/10.5194/acp-22-10077-2022>
- Hodshire, A. L., Lawler, M. J., Zhao, J., Ortega, J., Jen, C., Yli-Juuti, T., et al. (2016). Multiple new-particle growth pathways observed at the US DOE Southern Great Plains field site. *Atmospheric Chemistry and Physics*, 16(14), 9321–9348. <https://doi.org/10.5194/acp-16-9321-2016>
- Jokinen, T., Sipilä, M., Richters, S., Kerminen, V. M., Paasonen, P., Stratmann, F., et al. (2014). Rapid autoxidation forms highly oxidized RO<sub>2</sub> radicals in the atmosphere. *Angewandte Chemie-International Edition*, 53(52), 14596–14600. <https://doi.org/10.1002/anie.201408566>
- Katz, D. J., Abdelhamid, A., Stark, H., Canagaratna, M. R., Worsnop, D. R., & Browne, E. C. (2023). Chemical identification of new particle formation and growth precursors through positive matrix factorization of ambient ion measurements. *Atmospheric Chemistry and Physics*, 23(9), 5567–5585. <https://doi.org/10.5194/acp-23-5567-2023>
- Kirkby, J., Amorim, A., Baltensperger, U., Carslaw, K. S., Christoudias, T., Curtius, J., et al. (2023). Atmospheric new particle formation from the CERN CLOUD experiment. *Nature Geoscience*, 16(11), 948–957. <https://doi.org/10.1038/s41561-023-01305-0>
- Kulmala, M., Vehkamäki, H., Petaja, T., Dal Maso, M., Lauri, A., Kerminen, V. M., et al. (2004). Formation and growth rates of ultrafine atmospheric particles: A review of observations. *Journal of Aerosol Science*, 35(2), 143–176. <https://doi.org/10.1016/j.jaerosci.2003.10.003>
- Lee, S.-H., Uin, J., Guenther, A. B., de Gouw, J. A., Yu, F., Nadykto, A. B., et al. (2016). Isoprene suppression of new particle formation: Potential mechanisms and implications. *Journal of Geophysical Research: Atmospheres*, 121(24), 14621–14635. <https://doi.org/10.1002/2016JD024844>
- Li, X., & Bourq, I. C. (2023). Phase state, surface tension, water activity, and accommodation coefficient of water–organic clusters near the critical size for atmospheric new particle formation. *Environmental Science & Technology*, 57(35), 13092–13103. <https://doi.org/10.1021/acs.est.2c09627>
- Li, Y., Ji, Y., Zhao, J., Wang, Y., Shi, Q., Peng, J., et al. (2021). Unexpected oligomerization of small  $\alpha$ -dicarbonyls for secondary organic aerosol and brown carbon formation. *Environmental Science & Technology*, 55(8), 4430–4439. <https://doi.org/10.1021/acs.est.0c08066>
- Li, Y., Shen, J., Zhao, B., Cai, R., Wang, S., Gao, Y., et al. (2023). A dynamic parameterization of sulfuric acid–dimethylamine nucleation and its application in three-dimensional modeling. *Atmospheric Chemistry and Physics*, 23(15), 8789–8804. <https://doi.org/10.5194/acp-23-8789-2023>
- Mao, J., Yu, F., Zhang, Y., An, J., Wang, L., Zheng, J., et al. (2018). High-resolution modeling of gaseous methylamines over a polluted region in China: Source-dependent emissions and implications of spatial variations. *Atmospheric Chemistry and Physics*, 18(11), 7933–7950. <https://doi.org/10.5194/acp-18-7933-2018>
- McDonald, B. C., de Gouw, J. A., Gilman, J. B., Jathar, S. H., Akherati, A., Cappa, C. D., et al. (2018). Volatile chemical products emerging as largest petrochemical source of urban organic emissions. *Science*, 359(6377), 760–764. <https://doi.org/10.1126/science.aag0524>
- Molteni, U., Bianchi, F., Klein, F., El Haddad, I., Frege, C., Rossi, M. J., et al. (2018). Formation of highly oxygenated organic molecules from aromatic compounds. *Atmospheric Chemistry and Physics*, 18(3), 1909–1921. <https://doi.org/10.5194/acp-18-1909-2018>
- Murphy, B. N., Sonntag, D., Seltzer, K. M., Pye, H. O. T., Allen, C., Murray, E., et al. (2023). Reactive organic carbon air emissions from mobile sources in the United States. *Atmospheric Chemistry and Physics*, 23(20), 13469–13483. <https://doi.org/10.5194/acp-23-13469-2023>
- Ng, N. L., Kroll, J. H., Chan, A. W. H., Chhabra, P. S., Flagan, R. C., & Seinfeld, J. H. (2007). Secondary organic aerosol formation from *m*-xylene, toluene, and benzene. *Atmospheric Chemistry and Physics*, 7(14), 3909–3922. <https://doi.org/10.5194/acp-7-3909-2007>
- O'Donnell, S. E., Akherati, A., He, Y., Hodshire, A. L., Shilling, J. E., Kuang, C., et al. (2023). Look up: Probing the vertical profile of new particle formation and growth in the planetary boundary layer with models and observations. *Journal of Geophysical Research: Atmospheres*, 128(3), e2022JD037525. <https://doi.org/10.1029/2022JD037525>
- Olin, M., Okuljar, M., Rissanen, M. P., Kalliokoski, J., Shen, J., Dada, L., et al. (2022). Measurement report: Atmospheric new particle formation in a coastal agricultural site explained with binPMF analysis of nitrate CI-API-TOF spectra. *Atmospheric Chemistry and Physics*, 22(12), 8097–8115. <https://doi.org/10.5194/acp-22-8097-2022>
- Pennington, E. A., Seltzer, K. M., Murphy, B. N., Qin, M. M., Seinfeld, J. H., & Pye, H. O. T. (2021). Modeling secondary organic aerosol formation from volatile chemical products. *Atmospheric Chemistry and Physics*, 21(24), 18247–18261. <https://doi.org/10.5194/acp-21-18247-2021>
- Petäjä, T., Tabakova, K., Manninen, A., Ezhova, E., O'Connor, E., Moiseev, D., et al. (2022). Influence of biogenic emissions from boreal forests on aerosol–cloud interactions. *Nature Geoscience*, 15(1), 42–47. <https://doi.org/10.1038/s41561-021-00876-0>
- Rasool, Q. Z., Shrivastava, M., Octaviani, M., Zhao, B., Gaudet, B., & Liu, Y. (2021). Modeling volatility-based aerosol phase state predictions in the Amazon rainforest. *ACS Earth and Space Chemistry*, 5(10), 2910–2924. <https://doi.org/10.1021/acsearthspacechem.1c00255>
- Riipinen, I., Pierce, J. R., Yli-Juuti, T., Nieminen, T., Häkkinen, S., Ehn, M., et al. (2011). Organic condensation: A vital link connecting aerosol formation to cloud condensation nuclei (CCN) concentrations. *Atmospheric Chemistry and Physics*, 11(8), 3865–3878. <https://doi.org/10.5194/acp-11-3865-2011>
- Rissanen, M. (2021). Anthropogenic volatile organic compound (AVOC) autoxidation as a source of highly oxygenated organic molecules (HOM). *Journal of Physical Chemistry A*, 125(41), 9027–9039. <https://doi.org/10.1021/acs.jpca.1c06465>
- Rissanen, M. P., Kurten, T., Sipilä, M., Thornton, J. A., Kangasluoma, J., Sarnela, N., et al. (2014). The formation of highly oxidized multifunctional products in the ozonolysis of cyclohexene. *Journal of the American Chemical Society*, 136(44), 15596–15606. <https://doi.org/10.1021/ja507146s>
- Robinson, A. L., Donahue, N. M., Shrivastava, M. K., Weitkamp, E. A., Sage, A. M., Grieshop, A. P., et al. (2007). Rethinking organic aerosols: Semivolatile emissions and photochemical aging. *Science*, 315(5816), 1259–1262. <https://doi.org/10.1126/science.1133061>
- Saliba, G., Bell, D. M., Suski, K. J., Fast, J. D., Imre, D., Kulkarni, G., et al. (2023). Aircraft measurements of single particle size and composition reveal aerosol size and mixing state dictate their activation into cloud droplets. *Environmental Science: Atmospheres*, 3(9), 1352–1364. <https://doi.org/10.1039/D3EA00052D>
- Schervish, M., & Donahue, N. M. (2020). Peroxy radical chemistry and the volatility basis set. *Atmospheric Chemistry and Physics*, 20(2), 1183–1199. <https://doi.org/10.5194/acp-20-1183-2020>
- Schervish, M., Heinritzi, M., Stolzenburg, D., Dada, L., Wang, M., Ye, Q., et al. (2024). Interactions of peroxy radicals from monoterpene and isoprene oxidation simulated in the radical volatility basis set. *Environmental Science: Atmospheres*, 4(7), 740–753. <https://doi.org/10.1039/D4EA00056K>
- Schobesberger, S., D'Ambro, E. L., Vettikkat, L., Lee, B. H., Peng, Q., Bell, D. M., et al. (2023). Airborne flux measurements of ammonia over the southern Great Plains using chemical ionization mass spectrometry. *Atmospheric Measurement Techniques*, 16(2), 247–271. <https://doi.org/10.5194/amt-16-247-2023>
- Seinfeld, J. H., Bretherton, C., Carslaw, K. S., Coe, H., DeMott, P. J., Dunlea, E. J., et al. (2016). Improving our fundamental understanding of the role of aerosol–cloud interactions in the climate system. *Proceedings of the National Academy of Sciences*, 113(21), 5781–5790. <https://doi.org/10.1073/pnas.1514043113>

- Seltzer, K. M., Pennington, E., Rao, V., Murphy, B. N., Strum, M., Isaacs, K. K., & Pye, H. O. T. (2021). Reactive organic carbon emissions from volatile chemical products. *Atmospheric Chemistry and Physics*, 21(6), 5079–5100. <https://doi.org/10.5194/acp-21-5079-2021>
- Shetty, N., Liu, P., Liang, Y., Sumlin, B., Daube, C., Herndon, S., et al. (2023). Brown carbon absorptivity in fresh wildfire smoke: Associations with volatility and chemical compound groups. *Environmental Science: Atmospheres*, 3(9), 1262–1271. <https://doi.org/10.1039/D3EA00067B>
- Shrivastava, M., Andreae, M. O., Artaxo, P., Barbosa, H. M. J., Berg, L. K., Brito, J., et al. (2019). Urban pollution greatly enhances formation of natural aerosols over the Amazon rainforest. *Nature Communications*, 10(1), 1046. <https://doi.org/10.1038/s41467-019-08909-4>
- Shrivastava, M., Cappa, C. D., Fan, J., Goldstein, A. H., Guenther, A. B., Jimenez, J. L., et al. (2017). Recent advances in understanding secondary organic aerosol: Implications for global climate forcing. *Reviews of Geophysics*, 55(2), 509–559. <https://doi.org/10.1002/2016RG000540>
- Shrivastava, M., Easter, R. C., Liu, X., Zelenyuk, A., Singh, B., Zhang, K., et al. (2015). Global transformation and fate of SOA: Implications of low-volatility SOA and gas-phase fragmentation reactions. *Journal of Geophysical Research: Atmospheres*, 120(9), 4169–4195. <https://doi.org/10.1002/2014JD022563>
- Shrivastava, M., Fan, J., Zhang, Y., Rasool, Q. Z., Zhao, B., Shen, J., et al. (2024). Intense formation of secondary ultrafine particles from Amazonian vegetation fires and their invigoration of deep clouds and precipitation. *One Earth*, 7(6), 1029–1043. <https://doi.org/10.1016/j.oneear.2024.05.015>
- Shrivastava, M., Fast, J., Easter, R., Gustafson, W. I., Jr., Zaveri, R. A., Jimenez, J. L., et al. (2011). Modeling organic aerosols in a megacity: Comparison of simple and complex representations of the volatility basis set approach. *Atmospheric Chemistry and Physics*, 11(13), 6639–6662. <https://doi.org/10.5194/acp-11-6639-2011>
- Shrivastava, M., Rasool, Q. Z., Zhao, B., Octaviani, M., Zaveri, R. A., Zelenyuk, A., et al. (2022). Tight coupling of surface and in-plant biochemistry and convection governs key fine particulate components over the Amazon rainforest. *ACS Earth and Space Chemistry*, 6(2), 380–390. <https://doi.org/10.1021/acsearthspacechem.1c00356>
- Shrivastava, M., Zhao, C., Easter, R. C., Qian, Y., Zelenyuk, A., Fast, J. D., et al. (2016). Sensitivity analysis of simulated SOA loadings using a variance-based statistical approach. *Journal of Advances in Modeling Earth Systems*, 8(2), 499–519. <https://doi.org/10.1002/2015MS000554>
- Uin, J., Aiken, A. C., Dubey, M. K., Kuang, C. A., Pekour, M., Salwen, C., et al. (2019). Atmospheric radiation measurement (ARM) aerosol observing systems (AOS) for surface-based in situ atmospheric aerosol and trace gas measurements. *Journal of Atmospheric and Oceanic Technology*, 36(12), 2429–2447. <https://doi.org/10.1175/jtech-d-19-0077.1>
- Wang, J., Shilling, J. E., Liu, J., Zelenyuk, A., Bell, D. M., Petters, M. D., et al. (2019). Cloud droplet activation of secondary organic aerosol is mainly controlled by molecular weight, not water solubility. *Atmospheric Chemistry and Physics*, 19(2), 941–954. <https://doi.org/10.5194/acp-19-941-2019>
- Wang, M., Chen, D., Xiao, M., Ye, Q., Stolzenburg, D., Hofbauer, V., et al. (2020). Photo-oxidation of aromatic hydrocarbons produces low-volatility organic compounds. *Environmental Science & Technology*, 54(13), 7911–7921. <https://doi.org/10.1021/acs.est.0c02100>
- Wang, S. N., Wu, R. R., Berndt, T., Ehn, M., & Wang, L. M. (2017). Formation of highly oxidized radicals and multifunctional products from the atmospheric oxidation of alkylbenzenes. *Environmental Science & Technology*, 51(15), 8442–8449. <https://doi.org/10.1021/acs.est.7b02374>
- Xiao, M., Hoyle, C. R., Dada, L., Stolzenburg, D., Kürten, A., Wang, M., et al. (2021). The driving factors of new particle formation and growth in the polluted boundary layer. *Atmospheric Chemistry and Physics*, 21(18), 14275–14291. <https://doi.org/10.5194/acp-21-14275-2021>
- Yin, R., Yan, C., Cai, R., Li, X., Shen, J., Lu, Y., et al. (2021). Acid–base clusters during atmospheric new particle formation in urban Beijing. *Environmental Science & Technology*, 55(16), 10994–11005. <https://doi.org/10.1021/acs.est.1c02701>
- Zaveri, R. A., Easter, R. C., Fast, J. D., & Peters, L. K. (2008). Model for Simulating Aerosol Interactions and Chemistry (MOSAIC). *Journal of Geophysical Research*, 113(D13), D13204. <https://doi.org/10.1029/2007JD008782>
- Zaveri, R. A., Easter, R. C., Shilling, J. E., & Seinfeld, J. H. (2014). Modeling kinetic partitioning of secondary organic aerosol and size distribution dynamics: Representing effects of volatility, phase state, and particle-phase reaction. *Atmospheric Chemistry and Physics*, 14(10), 5153–5181. <https://doi.org/10.5194/acp-14-5153-2014>
- Zaveri, R. A., Wang, J., Fan, J., Zhang, Y., Shilling, J. E., Zelenyuk, A., et al. (2022). Rapid growth of anthropogenic organic nanoparticles greatly alters cloud life cycle in the Amazon rainforest. *Science Advances*, 8(2), eabj0329. <https://doi.org/10.1126/sciadv.abj0329>
- Zhang, J., Shrivastava, M., Zelenyuk, A., Zaveri, R. A., Surratt, J. D., Riva, M., et al. (2023). Observationally constrained modeling of the reactive uptake of isoprene-derived epoxydiols under elevated relative humidity and varying acidity of seed aerosol conditions. *ACS Earth and Space Chemistry*, 7(4), 788–799. <https://doi.org/10.1021/acsearthspacechem.2c00358>
- Zhang, R., Khalizov, A., Wang, L., Hu, M., & Xu, W. (2012). Nucleation and growth of nanoparticles in the atmosphere. *Chemical Reviews*, 112(3), 1957–2011. <https://doi.org/10.1021/cr2001756>
- Zhao, B., Fast, J. D., Donahue, N. M., Shrivastava, M., Schervish, M., Shilling, J. E., et al. (2021). Impact of urban pollution on organic-mediated new-particle formation and particle number concentration in the Amazon rainforest. *Environmental Science & Technology*, 55(8), 4357–4367. <https://doi.org/10.1021/acs.est.0c07465>
- Zhao, B., Shrivastava, M., Donahue, N. M., Gordon, H., Schervish, M., Shilling, J. E., et al. (2020). High concentration of ultrafine particles in the Amazon free troposphere produced by organic new particle formation. *Proceedings of the National Academy of Sciences*, 117(41), 25344–25351. <https://doi.org/10.1073/pnas.2006716117>
- Zhao, C., Huang, M. Y., Fast, J. D., Berg, L. K., Qian, Y., Guenther, A., et al. (2016). Sensitivity of biogenic volatile organic compounds to land surface parameterizations and vegetation distributions in California. *Geoscientific Model Development*, 9(5), 1959–1976. <https://doi.org/10.5194/gmd-9-1959-2016>

## References From the Supporting Information

- Abdul-Razzak, H., & Ghan, S. J. (2002). A parameterization of aerosol activation - 3. Sectional representation. *Journal of Geophysical Research*, 107(D3), AAC 1-1–AAC 1-6. <https://doi.org/10.1029/2001jd000483>
- Berg, L. K., Shrivastava, M., Easter, R. C., Fast, J. D., Chapman, E. G., Liu, Y., & Ferrare, R. A. (2015). A new WRF-Chem treatment for studying regional-scale impacts of cloud processes on aerosol and trace gases in parameterized cumuli. *Geoscientific Model Development*, 8(2), 409–429. <https://doi.org/10.5194/gmd-8-409-2015>
- Boyd, C. M., Sanchez, J., Xu, L., Eugene, A. J., Nah, T., Tuet, W. Y., et al. (2015). Secondary organic aerosol formation from the  $\beta$ -pinene+NO<sub>3</sub> system: Effect of humidity and peroxy radical fate. *Atmospheric Chemistry and Physics*, 15(13), 7497–7522. <https://doi.org/10.5194/acp-15-7497-2015>
- Canonaco, F., Crippa, M., Slowik, J. G., Baltensperger, U., & Prévôt, A. S. H. (2013). SoFi, an IGOR-based interface for the efficient use of the generalized multilinear engine (ME-2) for the source apportionment: ME-2 application to aerosol mass spectrometer data. *Atmospheric Measurement Techniques*, 6(12), 3649–3661. <https://doi.org/10.5194/amt-6-3649-2013>

- Chan, A. W. H., Chan, M. N., Surratt, J. D., Chhabra, P. S., Loza, C. L., Crounse, J. D., et al. (2010). Role of aldehyde chemistry and NO<sub>x</sub> concentrations in secondary organic aerosol formation. *Atmospheric Chemistry and Physics*, 10(15), 7169–7188. <https://doi.org/10.5194/acp-10-7169-2010>
- Chen, Q., Liu, Y., Donahue, N. M., Shilling, J. E., & Martin, S. T. (2011). Particle-phase chemistry of secondary organic material: Modeled compared to measured O:C and H:C elemental ratios provide constraints. *Environmental Science & Technology*, 45(11), 4763–4770. <https://doi.org/10.1021/es104398s>
- De Haan, D. O., Jimenez, N. G., de Loera, A., Cazaunau, M., Gratien, A., Pangui, E., & Doussin, J.-F. (2018). Methylglyoxal uptake coefficients on aqueous aerosol surfaces. *The Journal of Physical Chemistry A*, 122(21), 4854–4860. <https://doi.org/10.1021/acs.jpca.8b00533>
- Easter, R. C., Ghan, S. J., Zhang, Y., Saylor, R. D., Chapman, E. G., Laulainen, N. S., et al. (2004). MIRAGE: Model description and evaluation of aerosols and trace gases. *Journal of Geophysical Research*, 109(D20), D20210. <https://doi.org/10.1029/2004jd004571>
- Ervens, B., & Volkamer, R. (2010). Glyoxal processing by aerosol multiphase chemistry: Towards a kinetic modeling framework of secondary organic aerosol formation in aqueous particles. *Atmospheric Chemistry and Physics*, 10(17), 8219–8244. <https://doi.org/10.5194/acp-10-8219-2010>
- Gaston, C. J., Riedel, T. P., Zhang, Z. F., Gold, A., Surratt, J. D., & Thornton, J. A. (2014). Reactive uptake of an isoprene-derived epoxydiol to submicron aerosol particles. *Environmental Science & Technology*, 48(19), 11178–11186. <https://doi.org/10.1021/es5034266>
- Ge, X., Sun, Y., Trousdell, J., Chen, M., & Zhang, Q. (2023). Enhancing characterization of organic nitrogen components in aerosols and droplets using high-resolution aerosol mass spectrometry. *EGU sphere*, 2023, 1–25.
- Guenther, A. B., Jiang, X., Heald, C. L., Sakulyanontvittaya, T., Duhl, T., Emmons, L. K., & Wang, X. (2012). The Model of Emissions of Gases and Aerosols from Nature version 2.1 (MEGAN2.1): An extended and updated framework for modeling biogenic emissions. *Geoscientific Model Development*, 5(6), 1471–1492. <https://doi.org/10.5194/gmd-5-1471-2012>
- Iacono, M. J., Delamere, J. S., Mlawer, E. J., Shephard, M. W., Clough, S. A., & Collins, W. D. (2008). Radiative forcing by long-lived greenhouse gases: Calculations with the AER radiative transfer models. *Journal of Geophysical Research*, 113(D13), D13103. <https://doi.org/10.1029/2008jd009944>
- Janeček, N. J., Hansen, K. M., & Stanier, C. O. (2017). Comprehensive atmospheric modeling of reactive cyclic siloxanes and their oxidation products. *Atmospheric Chemistry and Physics*, 17(13), 8357–8370. <https://doi.org/10.5194/acp-17-8357-2017>
- Kleindienst, T. E., Lewandowski, M., Offenberg, J. H., Jaoui, M., & Edney, E. O. (2007). Ozone-isoprene reaction: Re-examination of the formation of secondary organic aerosol. *Geophysical Research Letters*, 34(1), L01805. <https://doi.org/10.1029/2006GL027485>
- Kroll, J. H., Ng, N. L., Murphy, S. M., Flagan, R. C., & Seinfeld, J. H. (2006). Secondary organic aerosol formation from isoprene photooxidation. *Environmental Science & Technology*, 40(6), 1869–1877. <https://doi.org/10.1021/es0524301>
- Li, Y., Shen, J., Zhao, B., Cai, R., Wang, S., Gao, Y., et al. (2023). A parameterization of sulfuric acid-dimethylamine nucleation and its application in three-dimensional modeling. *Atmospheric Chemistry and Physics Discussions*, 2023, 1–22.
- Liggio, J., Li, S.-M., & McLaren, R. (2005). Reactive uptake of glyoxal by particulate matter. *Journal of Geophysical Research*, 110(D10), D10304. <https://doi.org/10.1029/2004JD005113>
- Liu, J., Alexander, L., Fast, J. D., Lindenmaier, R., & Shilling, J. E. (2021). Aerosol characteristics at the Southern Great Plains site during the HI-SCALE campaign. *Atmospheric Chemistry and Physics*, 21(6), 5101–5116. <https://doi.org/10.5194/acp-21-5101-2021>
- Lu, Q., Murphy, B. N., Qin, M., Adams, P. J., Zhao, Y., Pye, H. O. T., et al. (2020). Simulation of organic aerosol formation during the CalNex study: Updated mobile emissions and secondary organic aerosol parameterization for intermediate-volatility organic compounds. *Atmospheric Chemistry and Physics*, 20(7), 4313–4332. <https://doi.org/10.5194/acp-20-4313-2020>
- Ng, N. L., Chhabra, P. S., Chan, A. W. H., Surratt, J. D., Kroll, J. H., Kwan, A. J., et al. (2007). Effect of NO<sub>x</sub> level on secondary organic aerosol (SOA) formation from the photooxidation of terpenes. *Atmospheric Chemistry and Physics*, 7(19), 5159–5174. <https://doi.org/10.5194/acp-7-5159-2007>
- Ng, N. L., Kwan, A. J., Surratt, J. D., Chan, A. W. H., Chhabra, P. S., Sorooshian, A., et al. (2008). Secondary organic aerosol (SOA) formation from reaction of isoprene with nitrate radicals (NO<sub>3</sub>). *Atmospheric Chemistry and Physics*, 8(14), 4117–4140. <https://doi.org/10.5194/acp-8-4117-2008>
- Paatero, P. (1999). The multilinear engine - A table-driven, least squares program for solving multilinear problems, including the *n*-way parallel factor analysis model. *Journal of Computational & Graphical Statistics*, 8(4), 854–888. <https://doi.org/10.2307/1390831>
- Qin, M. M., Murphy, B. N., Isaacs, K. K., McDonald, B. C., Lu, Q. Y., McKeen, S. A., et al. (2021). Criteria pollutant impacts of volatile chemical products informed by near-field modelling. *Nature Sustainability*, 4(2), 129–137. <https://doi.org/10.1038/s41893-020-00614-1>
- Rolph, G., Stein, A., & Stunder, B. (2017). Real-time Environmental Applications and Display sYstem: READY. *Environmental Modelling & Software*, 95, 210–228. <https://doi.org/10.1016/j.envsoft.2017.06.025>
- Seltzer, K. M., Murphy, B. N., Pennington, E. A., Allen, C., Talgo, K., & Pye, H. O. T. (2022). Volatile chemical product enhancements to criteria pollutants in the United States. *Environmental Science & Technology*, 56(11), 6905–6913. <https://doi.org/10.1021/acs.est.1c04298>
- Shilling, J. E., Chen, Q., King, S. M., Rosenoern, T., Kroll, J. H., Worsnop, D. R., et al. (2008). Particle mass yield in secondary organic aerosol formed by the dark ozonolysis of  $\alpha$ -pinene. *Atmospheric Chemistry and Physics*, 8(7), 2073–2088. <https://doi.org/10.5194/acp-8-2073-2008>
- Stein, A. F., Draxler, R. R., Rolph, G. D., Stunder, B. J. B., Cohen, M. D., & Ngan, F. (2015). NOAA's HYSPLIT atmospheric transport and dispersion modeling system. *Bulletin of the American Meteorological Society*, 96(12), 2059–2077. <https://doi.org/10.1175/bams-d-14-00110.1>
- Vaden, T. D., Imre, D., Beránek, J., Shrivastava, M., & Zelenyuk, A. (2011). Evaporation kinetics and phase of laboratory and ambient secondary organic aerosol. *Proceedings of the National Academy of Sciences of the United States of America*, 108(6), 2190–2195. <https://doi.org/10.1073/pnas.1013391108>
- Zhao, J., Levitt, N. P., Zhang, R., & Chen, J. (2006). Heterogeneous reactions of methylglyoxal in acidic media: Implications for secondary organic aerosol formation. *Environmental Science & Technology*, 40(24), 7682–7687. <https://doi.org/10.1021/es060610k>